Monthly Notices of the ROYAL ASTRONOMICAL SOCIETY

MNRAS **546,** 1–21 (2026) https://doi.org/10.1093/mnras/staf2278
Advance Access publication 2025 December 30

A young supernova selection pipeline for the LSST era

Harry Addison [1]★ Chris Frohmaier [2] Kate Maguire [3] Robert C. Nichol,[1] Isobel Hook [4] and Stephen J. Smartt [5,6]

[1]*Department of Physics, University of Surrey, Guildford GU2 7XH, UK*
[2]*Institute of Cosmology and Gravitation, University of Portsmouth, Portsmouth PO1 3FX, UK*
[3]*School of Physics, Trinity College Dublin, The University of Dublin, Dublin 2 D02 PN40, Ireland*
[4]*Department of Physics, Lancaster University, Lancaster, Lancashire LA1 4YB, UK*
[5]*Department of Physics, University of Oxford, Keble Road, Oxford OX1 3RH, UK*
[6]*Astrophysics Research Centre, School of Mathematics and Physics, Queen's University Belfast, Belfast BT7 1NN, UK*

Accepted 2025 December 19. Received 2025 November 17; in original form 2024 December 6

ABSTRACT

Early-time spectroscopy of supernovae (SNe), acquired within days of explosion, yields crucial insights into their outermost ejecta layers, facilitating the study of their environments, progenitor systems, and explosion mechanisms. Recent efforts in early discovery and follow-up of SNe have shown the potential insights that can be gained from early-time spectra. Surveys such as the Time-Domain Extragalactic Survey (TiDES), conducted with the 4m Multi-Object Spectroscopic Telescope (4MOST), will provide spectroscopic follow-up of transients discovered by the Legacy Survey of Space and Time (LSST). Current simulations indicate that early-time spectroscopic studies conducted with TiDES data will be limited by the current SN selection criteria. To enhance early-time SN spectroscopic studies from TiDES-like surveys, we propose a set of selection criteria focusing on young SNe (YSNe), which we define as SNe prior to −10 days before peak brightness. Utilizing the Zwicky Transient Facility transient alerts, we developed criteria to select YSNe while minimizing the sample's contamination rate to 23 per cent. The developed criteria were applied to LSST simulations, yielding a sample of 694 Deep Drilling Field survey SNe and 56260 Wide Fast Deep survey SNe for follow-up. We demonstrate that our criteria enables the selection of SNe at early-times, enhancing future early-time spectroscopic SN studies from TiDES-like surveys. Finally, we investigated 4MOST-like observing strategies to increase the sample of spectroscopically observed YSNe. We propose that a 4MOST-like observing strategy that follows LSST with a delay of 3 days is optimal for a TiDES-like SN survey in terms of the number of classifiable spectra obtained, while a 1 day delay is most optimal for enhancing the early-time science in conjunction with our YSN selection criteria.

Key words: techniques: photometric – techniques: spectroscopic – surveys – transients: supernovae.

1 INTRODUCTION

Supernovae (SNe) are a diverse set of transients with many different progenitor scenarios and explosion mechanisms. For the case of thermonuclear (Type Ia) supernovae, there are two traditional progenitor scenarios [single-degenerate scenario (J. Whelan & J. Iben 1973) and double-degenerate scenario (J. Iben & A. V. Tutukov 1984)], while there are many different explosion mechanisms being studied, which include pure deflagration models (K. Nomoto, F. K. Thielemann & K. Yokoi 1984; G. C. Jordan et al. 2012; M. Kromer et al. 2013; M. Fink et al. 2014; F. Lach et al. 2022), deflagration-to-detonation (delayed-detonation) models (W. D. Arnett 1969; A. M. Khokhlov 1991; V. N. Gamezo, A. M. Khokhlov & E. S. Oran 2005; F. K. Röpke & J. C. Niemeyer 2007; I. Rabinak, E. Livne & E. Waxman 2012; I. R. Seitenzahl et al. 2013), double-detonation models (M. Fink, W. Hillebrandt & F. K. Röpke 2007; M. Fink et al. 2010; M. Kromer et al. 2010; K. J. Shen & K. Moore 2014; A. Polin, P. Nugent & D. Kasen 2019; M. R. Magee et al. 2021; S. J. Boos, D. M. Townsley & K. J. Shen 2024), core-degenerate explosions (N. Soker 2013; B. Wang et al. 2017), triple collision models (D. Kushnir et al. 2013; N. Hallakoun & D. Maoz 2019), and rotating super-Chandrasekhar mass explosions (R. Di Stefano, R. Voss & J. S. W. Claeys 2011).

To investigate the explosion mechanisms of SNe Ia, previous studies have investigated the early light curves of SN Ia events (A. G. Riess et al. 1999; B. T. Hayden et al. 2010; F. B. Bianco et al. 2011; M. Ganeshalingam, W. Li & A. V. Filippenko 2011; R. E. Firth et al. 2015; A. A. Miller et al. 2020; M. Deckers et al. 2022; J. Burke et al. 2022a, b; M. M. Fausnaugh et al. 2023; Y. Q. Ni et al. 2025). In addition to early-time photometry, early-time spectroscopy can further provide us with a wealth of information about the explosion dynamics. Spectra taken within a few days of explosion allow us to trace the outermost layers of the ejecta. From these spectra, we can determine the chemical abundances of the outer layers, which can then be used to distinguish between explosion models (M. R. Magee et al. 2021; M. Ogawa, K. Maeda & M. Kawabata 2023). Early-time spectra can also be used to study SNe Ia that display a 'bump' in their pre-peak light curves, which is thought to be the

★ E-mail: ha00871@surrey.ac.uk

result of the shock front interacting with the binary companion (D. Kasen 2010), or from the presence of short-lived radioactive isotopes (U. M. Noebauer et al. 2017).

Furthermore, early-time spectra are not only useful for studying thermonuclear SN explosion mechanisms, but they can also be used to study core collapse (CC) SNe. Early-time spectra can be used to investigate the progenitor systems of CC SNe by providing us with the ability to constrain the progenitor's chemical abundance, wind speed, and mass-loss (A. Pastorello et al. 2007; N. Smith et al. 2007, 2023; E. A. Zimmerman et al. 2024). As with SNe Ia, some CC SNe also exhibit a 'bump' in their pre-peak light curves, which is caused by an interaction of the shock front with circumstellar material (CSM; A. L. Piro & V. S. Morozova 2016; A. Gagliano et al. 2022; A. Kozyreva et al. 2022). Spectra taken within hours to days of explosion, known as flash spectroscopy, can reveal narrow emission lines from the shock breakout flash-ionization and recombination of the CSM, offering a direct probe of the progenitor's immediate environment and final stages of mass-loss (A. Gal-Yam et al. 2014; D. Khazov et al. 2016; O. Yaron et al. 2017; C. S. Kochanek 2019; R. J. Bruch et al. 2023; W. V. Jacobson-Galán et al. 2023; E. A. Zimmerman et al. 2024).

Besides the study of SN progenitors and explosion mechanisms, early-time spectra can also be very useful for classifications. Some types of SNe, such as stripped envelope SN that retain a small hydrogen envelope, can only be reliably classified from their early phase spectra (Y. Dong et al. 2024). Additionally, the ability to spectroscopically classify SNe early in their evolution allows us to conduct targeted observations of high interest SNe, such as the previously mentioned 'bump' SNe or other peculiar types.

Currently, our spectroscopic samples of SNe, and in particular early-time spectra, are restricted by the availability of spectroscopic resources that can quickly follow-up photometrically discovered transients. The *Zwicky Transient Facility* (ZTF; E. C. Bellm et al. 2019; F. J. Masci et al. 2019) is one of the leading facilities of transient astronomy, with its Northern Sky Survey observing the northern sky (declination $> -31^{\circ}$) every 2 days in both the g - and r-bands. This has allowed for the discovery of many transient events, however, a key part of ZTF's success is its *Bright Transient Survey* (BTS; C. Fremling et al. 2020). BTS uses an automated low resolution integral field unit spectrograph, the Spectral Energy Distribution Machine (S. Ben-Ami et al. 2012; N. Blagorodnova et al. 2018; M. Rigault et al. 2019), to compliment the Northern Sky Survey by providing spectroscopic follow-up of the ZTF discovered transients. The main aim of BTS is to provide a complete sample of spectroscopically classified extra-galactic transients within the Northern Sky Survey that are brighter than 18.5 mag (C. Fremling et al. 2020). Between June 2018 and April 2025, ZTF and BTS have found and spectroscopically classified over 10 600 SNe.[1]

In the coming years, the detection rates of transients will be greatly increased, with the Vera C. Rubin Observatory's *Legacy Survey of Space and Time* (LSST; Ž. Ivezić et al. 2019) discovering millions of SNe. Along with increased photometric observations of SNe, we will also see a large increase in our spectroscopic SN samples. The *Time-Domain Extragalactic Survey* (TiDES; E. Swann et al. 2019; C. Frohmaier et al. 2025) is one of the 25 surveys to be conducted on the *4m Multi-Object Spectroscopic Telescope* (4MOST; R. S. Jong et al. 2019), providing follow-up spectra of LSST transients. TiDES will operate over 5 years in parallel with the other 4MOST surveys, constructing the largest spectroscopic cosmological SN sample to date (C. Frohmaier et al. 2025, hereafter CF).

In order to obtain follow-up spectra of LSST transients, TiDES will select its targets by applying sets of selection criteria to the real time transient alerts that LSST will send out (CF). The different sets of selection criteria will be used in conjunction with one another to enhance the scientific output of TiDES. The current proposed selection criteria for SN are described by CF, and are as follows:

(i) Transient detected to $> 5\sigma$ in three or more bands.
(ii) Transient observed on two distinct nights.
(iii) Transient is brighter than 22.5 mag in any $griz$ filter.

Using simulations of LSST and 4MOST, CF showed that their current SN selection criteria predominantly selects pre-peak SNe from the LSST alerts. However, they also showed that there is on average a 7 d delay between the selection of a target from LSST and its subsequent follow-up using 4MOST. This results in many of the obtained SN spectra being taken during post-peak SN phases, with very few spectra obtained for phases (relative to peak brightness hereafter) before -15 d. Therefore, studies such as that of SN explosion mechanisms, progenitor compositions, wind speeds, mass-loss, and early-time CSM/binary companion interactions will be limited with the TiDES spectroscopic SN sample based on current plans.

In this study, we propose a new set of selection criteria for TiDES-like surveys that are focused on selecting transients as early as possible for the purpose of producing a SN sample for early-time astrophysical studies. Our criteria are designed to be used in conjunction with other selection criteria that are implemented within TiDES-like surveys, with a specific focus on enhancing the sample of young (early-time) SN (YSN) spectra. Throughout this study, we define a YSN as a SN at a phase prior to -10 d with respect to peak brightness. Whilst early selection is our primary objective, our selection criteria must also ensure that the YSN sample is not highly contaminated. This is due to the limited number of observing hours available for TiDES-like surveys that we do not want to waste on non-real sources. By using the ZTF transient alerts and LSST simulations, we aim to demonstrate that our proposed selection criteria will provide TiDES-like surveys with more early-time SN targets to follow-up than the current selection criteria, whilst minimizing the contamination.

Additionally, we investigate observing strategies with the aim of optimizing a 4MOST-like observing strategy for the use case of a TiDES-like SN survey and our YSN selection criteria. We explore different observing strategies to improve the quality of the obtained SN spectra, also considering the need for a quick follow-up of the targets in order to make full use of the early SN selection provided by our YSN selection criteria. We do not consider the impact that the investigated observing strategies have on the non-SN surveys when determining an optimal strategy. In this work our objective is not to produce a full 4MOST-like observing strategy, but rather to provide guidelines for future works towards developing and simulating 4MOST-like observing strategies.

This paper is organized as follows. In Section 2, we present the development of our YSN selection criteria using the ZTF transient alerts. In Section 3, we adapt and apply our developed selection criteria to an LSST simulation, presenting the resulting YSN candidate sample. The YSN candidate sample is then evaluated by comparing it to the SN sample produced by the current TiDES selection criteria. In Section 4, we investigate different 4MOST-like observing strategies, attempting to optimize the output of the TiDES-

[1]ZTF Bright Transient Survey, https://sites.astro.caltech.edu/ztf/bts/bts.php (accessed 13/06/2025)

Table 1. Developed YSN selection criteria for use on the ZTF transient alerts. Provided are the criteria along with a description of each criterion's purpose.

Criterion	Reasoning
g- or r-band magnitude < 22.5 mag [a]	Ensures that the object will meet the TiDES SN SSC
Galactic latitude $< -10^\circ$ OR Galactic latitude $> 10^\circ$	Removal of Galactic transient sources
Number of g- or r-band $> 5\sigma$ positive difference detections ≥ 2	Two or more $> 5\sigma$ g- or r-band detections required for brightening rate criterion
`Sherlock` classification not: VS, AGN, CV, BS	Removal of contaminants
Age < 7, 14 d [b]	Removes older objects that are unlikely pre-peak SNe
Brightening rate > 0.2, 0.1, 0.05 mag d^{-1} [b]	Removes dimming and slow brightening sources that are unlikely to be YSNe.

[a]This criterion has no effect when applied to ZTF transient alerts as ZTF only detects objects brighter than 21.5 mag.
[b]The multiple values provided are the values that were tested, and only one value for a given criterion was applied at any given time.

like surveys and our YSN selection criteria. Finally, in Section 5, we summarize the conclusions of this study.

2 YSN SELECTION CRITERIA DEVELOPMENT

Transient follow-up surveys such as TiDES will obtain targets from the live transient alerts that LSST will produce. As LSST is due to start operations in late 2025,[2] we must look to other means of developing and testing our selection criteria. One way in which this could be done is with the LSST simulations such as those used by CF, which simulate a SN population and their LSST photometric observations. However, one major limitation of these simulations is that they focus on the extragalactic Universe, excluding Galactic events (such as cataclysmic variables) that form a major source of contamination for a young and bright extragalactic transient search. Therefore, the LSST simulations used by CF do not fully represent the transient/variable sky that will be present in the live LSST transient alerts. As we want to produce a high purity (low contamination) YSN sample, as to not waste fibre hours (observing time) on non-real sources, using the LSST simulations alone is not enough to investigate this requirement. Therefore, we made use of the ZTF transient alerts, which will be similar to the LSST alerts, to develop and investigate suitable selection criteria that produce a high-purity YSN sample.

2.1 Proposed YSN selection criteria

ZTF has been observing the northern sky with a cadence of two d in the g- and r-filter bands since December 2020.[3] When a source is detected to vary above a specified detection threshold in the difference image, an alert is sent out to the wider community through brokers (M. T. Patterson et al. 2019). These alerts contain information about the source including, but not limited to; its object ID, coordinates, magnitude and filter band, associated detections from the last 30 d, and cutouts of science and difference images. Additionally, brokers provide their own data products to enhance the ZTF alerts. For example, the Lasair broker (K. W. Smith et al. 2019; R. D. Williams et al. 2024) supplies a contextual classification of the object using its contextual classifier, Sherlock (D. R. Young 2023). In this study, we adopted Lasair as our broker of choice, which is predominantly motivated by its use by TiDES for development purposes.

We considered the information provided in the ZTF alerts, along with additional data products provided by Lasair, and proposed a set of YSN selection criteria. These proposed criteria are presented in Table 1 along with a summary of the motivations behind using them, which are discussed in more detail below.

Our first proposed criterion, objects must be brighter than 22.5 mag in either the g- or r-band, was adopted from the current TiDES selection criteria. CF used this to ensure that a selected object is bright enough to meet the TiDES SN spectral success criteria (SSC), which is a criterion that defines whether or not an observation was successful. The SSC for TiDES SN is that for a given spectrum the mean signal-to-noise ratio (SNR) in the wavelength range 4500-8000 Å is more than 5 per 15 Å, which is based on the ability of SN classification tools to provide reliable classifications (CF). Therefore, we also require our objects to be brighter than 22.5 mag. It is worth mentioning that ZTF has a best case 5σ limit of $\sim$21.5 mag (E. C. Bellm et al. 2019), meaning that this criterion has no effect on the produced ZTF samples.

The second criterion, exclusion of objects between Galactic latitudes of -10° and 10°, was used to remove the Galactic plane from our selection region. We are only interested in extragalactic transients. Therefore, this criteria reduces the number of Galactic transients that are selected by our selection criteria.

Our next criterion, an object must have two or more positive difference detections greater than 5σ in the same band, is to exclude objects with a single or no positive detections in both the g- and r-bands. As is made clear in Section 2.2, by applying this criterion we reduced the computational resources and time required to apply our last two criteria.

Next we utilized `Sherlock` (D. R. Young 2023), a contextual classifier, to filter out objects that we considered as contamination such as variable stars (VS), active galactic nuclei (AGNs), cataclysmic variables (CV), and bright stars (BS). The classifier is not 100 per cent accurate, but we are not looking for a complete sample of YSNe, and our last two selection criteria are focused on removing any contaminants that remain.

Our penultimate criterion, referred to as the age constraint, is a constraint on the time since the first 5σ positive difference detection of an object. This was utilized to reduce the contamination of our selected YSN candidate sample by removing long-lived transients. The age constraint should also reduce the number of post peak SNe in the sample as it will remove SN that have been observed over longer periods of time, which are likely no longer early-time SNe. Unlike the previous criteria, the age criterion does not have a clear definitive threshold value, so we tested two values: 7 and 14 d.

[2]LSST project status, available at https://www.lsst.org/about/project-status (accessed 17/10/2024)
[3]ZTF public data release 5 notes, available at https://irsa.ipac.caltech.edu/data/ZTF/docs/releases/dr05/ztf_release_notes_dr05.pdf (accessed on 28/04/2025)

Our final criterion, a brightening rate constraint, was used to further remove contaminants from our YSN candidate sample. As the brightening rate of a SN in its early phases is generally much more rapid than at near-peak phases, we exploited this property to filter out 'slowly' brightening and dimming sources that are unlikely to be linked to the early phases of a SN outburst. To employ this criterion, we used equation (1) to calculate the brightening rate between the latest observation and the mean of the second latest night's observations of the same filter band:

$$\text{Brightening rate} = \frac{-(m_{\text{latest}} - m_{\text{night2}})}{\text{JD}_{\text{latest}} - \text{JD}_{\text{night2}}}, \quad (1)$$

where the brightening rate is in units of magnitudes per day (mag d^{-1}), m_{latest} is the apparent magnitude of the latest observation, m_{night2} is the mean magnitude of the previous available night's observations in the same filter band as the latest observation, $\text{JD}_{\text{latest}}$ is the Julian date (JD) of the latest observation, and $\text{JD}_{\text{night2}}$ is the average JD of the previous available night's observations in the same filter band as the latest observation. We associate a positive brightening rate with a source that is brightening, hence the use of the negative magnitude difference between the two nights ($m_{\text{latest}} - m_{\text{night2}}$) in equation (1). We compared the latest observation to the observations from the previous available night, as observations (of the same band) taken within the same night can vary in magnitude (but within error), which in some cases can cause a false sense of brightening or dimming between the consecutive observations. For the same reason, we took the mean of the g- or r-band observations on the previous available night.

As with the age criterion, the brightening rate does not have a definitive threshold value, and so we applied and tested three values: 0.05 mag d^{-1}, 0.1 mag d^{-1}, and 0.2 mag d^{-1}. For an object to be selected as a YSN, it had to have a brightening rate more positive than the mentioned values, which corresponds to a more rapid brightening than the threshold values.

2.2 Querying archived alerts and Lasair for transient data

In order to choose the most suitable values for the age and brightening rate criteria, as well as to evaluate our proposed YSN selection criteria, we produced YSN candidate samples by applying our criteria to the ZTF archived transient alerts.[4] We began by applying the magnitude, galactic latitude, and number of positive difference detection constraints to the alerts (the first three criteria in Table 1).

As the alerts do not contain enhancements by the brokers, to apply our Sherlock classification criteria, we queried Lasair for the Sherlock classifications of the objects that passed our initial filtering. This was achieved by using the table query method within Lasair's PYTHON API, which allows you to perform an SQL query on the Lasair database. Objects with Sherlock classifications of VS, AGN, CV, or BS were removed from the sample.

Next, we applied the age and brightening rate criteria by obtaining the light curves of the objects that remained in our sample. We made use of the light curve query method within Lasair's PYTHON API, which allows you to download the full light curve (detections and non-detections) of an object using its ZTF candidate ID. We then calculated the 'age' of the object and applied the age constraint to it, producing an 'age' restricted sample. For this sample of objects, the brightening rate was then calculated and the brightening rate criterion was applied to produce a YSN candidate sample.

2.3 YSN selection criteria testing

Throughout the development of our YSN selection criteria, six different YSN candidate samples were produced to test the different proposed age and brightening rate threshold values. The details of how these YSN candidate samples were produced, along with discussions of these samples for the purpose of development and evaluation of our criteria are provided in the sections that follow.

2.3.1 *Producing ZTF YSN candidate samples*

To select a suitable constraint values for the ambiguous age and brightening rate criteria, we first produced samples of objects by applying the methods outlined in Section 2.2 to the archived ZTF alerts. We selected archived alerts from a total of 60 nights split between a summer period (5 June–10 July 2023) and a winter period (10 December 2023 to 29 January 2024). These periods exceed a total of 60 nights as we did not select nights where ZTF did not observe. We note here that we excluded observations from the nights of 13–15 December 2023, as ZTF was performing an extragalactic high cadence experiment,[5] which is not representative of normal survey operations and could impact our results. As mentioned in Section 2.1, we tested two threshold values (7 and 14 d) for the age criterion, and three threshold values (0.05, 0.1, and 0.2 mag d^{-1}) for the brightening rate criterion. Therefore, we produced six samples, each produced from a different combination of the age and brightening rate criteria threshold values.

2.3.2 *Analysing ZTF YSN Candidate Samples*

To select the more optimized constraint values for our needs, we investigated the contamination (non-YSN objects) of the samples. This was accomplished by cross matching the objects to the *Transient Name Server* (TNS; IAU 2023), obtaining their classifications if possible. For the TNS classified SNe, we obtained the JD of peak brightness from the BTS sample explorer.[6] If a SN was not present in the BTS sample, then the JD of peak brightness was estimated by fitting a fourth degree polynomial to the g-band light curve if possible, otherwise the r-band light curve was used. The times of maximum from the polynomial fits have uncertainties in the range of 1–5 d, depending on the light curve sampling near maximum. The JD of peak brightness was used to calculate the phase at which a given SN was selected, and subsequently determine if it was a YSN (phase < -10 d), pre-peak SN (phase < 0 d), or post-peak SN (phase ≥ 0 d) at the time of selection. It should be noted that YSNe are a subset of pre-peak SNe.

Additionally, we further investigated the nature of the unclassified objects, as some of these objects could be unclassified SNe, and possibly YSNe. We visually inspected all of the unclassified objects' light curves resulting from our different selection criteria (1025 total objects), considering their shape, rise, time-scales, and evolution to determine if they were SN-like. If an object was deemed to be SN-like, we then estimated the date of peak brightness using the

[4] ZTF Alert Archive https://ztf.uw.edu/alerts/public/ (accessed on 13/05/2025).

[5] ZTF experiments, available at https://www.ztf.caltech.edu/ztf-experiments.html, (accessed on 21/05/2025)

[6] BTS sample explorer, available at https://sites.astro.caltech.edu/ztf/bts/explorer.php (accessed on 13/05/2025)

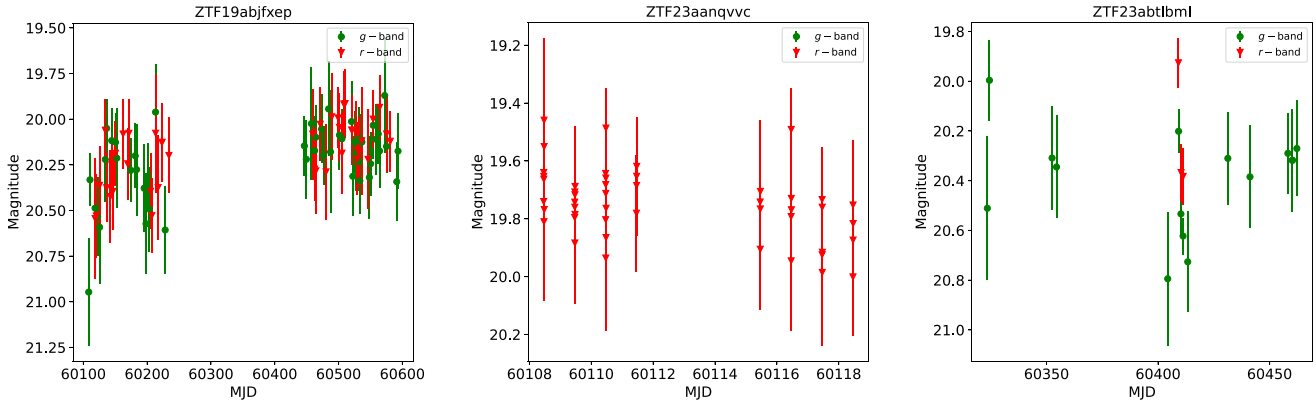

Figure 1. Light curves of unclassified contaminants in our YSN candidate sample selected from the ZTF transient alerts. (Left) g- and r-band light curves of a contaminant that is likely an AGN or quasar. (Middle and right) g- and r-band light curves of contaminants that have no clear nature.

Table 2. Six samples of objects that passed the selection criteria stated in Table 1, applying the different combinations (as stated) of age and brightening rate criterion thresholds. Provided are the TNS classifications of the objects, with the SNe being further classified based on if they were young, pre-peak, or post-peak at the time of selection. The unclassified objects were visually inspected, with the SN-like objects being further identified as being YSN-like, pre-peak SN-like, or post-peak SN-like. YSNe and YSN-like objects are a subset of pre-peak SNe and pre-peak SN-like objects, respectively. Also provided are the contamination rates of the samples, with one assuming non-YSNe as contaminants and the other assuming non-SNe as contaminants.

Criteria thresholds		Classification									Contamination	
Age	Brightening rate	YSNe	Pre-peak SNE	Post-peak SNE	TDE	Nova	Unclassified				Non-YSNe	Non-SNe
							Non-SNe [c]	YSNe [c]	Pre-Peak SNe [c]	Post-peak SNe [c]		
< 7 d	> 0.05 mag d^{-1}	79	179	10	2	1	308	51	443	36	87 per cent	32 per cent
< 14 d	> 0.05 mag d^{-1}	84	212	17	3	1	407	57	531	87	89 per cent	33 per cent
< 7 d	> 0.1 mag d^{-1}	74	149	2	1	1	172	37	307	14	83 per cent	27 per cent
< 14 d	> 0.1 mag d^{-1}	76	166	5	2	1	216	40	347	32	85 per cent	28 per cent
< 7 d	> 0.2 mag d^{-1}	60	97	1	1	1	58	17	100	6	71 per cent	23 per cent
< 14 d	> 0.2 mag d^{-1}	60	99	1	2	1	69	17	104	11	73 per cent	25 per cent

[c]Classifications based on visual inspection of the objects' light curves.

same polynomial fitting method previously described. As with the classified SNe, we use the date of peak brightness to determine if the SN-like object could be a YSN, a pre-peak SN, or a post-peak SN. Examples of non-SN contaminants in our YSN candidate samples are presented in Fig. 1. Approximately, 4 per cent of the contaminants are likely unclassified AGN or quasars (see left plot of Fig. 1). For 79 per cent of contaminants, their nature is unclear due to the lack of observations, with many light curves having fewer than 5 observations. The remaining 17 per cent of contaminants have reasonably sampled light curves but an unclear nature (see middle and right plots of Fig. 1).

Using the TNS classifications, the estimated dates of peak brightness for the SNe, and the results from our visual inspection of the unclassified objects, we calculated the contamination rate. As the aim of our YSN selection criteria is to select YSN, we considered all non-YSN objects to be contamination. Therefore, we calculated the contamination of a given sample as the percentage of non-YSN objects in the sample relative to the total number of objects in the sample. Additionally, we calculated and provide the contamination rate where only non-SN objects (TDE, novae, and the unclassified objects that were not deemed SN-like) are considered contaminants.

2.3.3 *ZTF YSN Candidate Samples*

Presented in Table 2 are the six YSN candidate samples produced from the proposed selection criteria with different combinations of the age and brightening rate criteria threshold values. The table displays the number of objects based on their TNS classifications, with the SNe being further determined to be YSNe, pre-peak SNe, or post-peak SNe. The number of unclassified objects is broken down further into non-SNe, YSNe, pre-peak SNe, or post-peak SNe, which is based on our visual inspection of the unclassified objects' light curves. Additionally, the table also provides the non-YSN contamination rates (percentage of the sample that is not a YSN) and non-SN contamination rates (percentage of the sample that is not a SN) of the samples. The non-YSN and non-SN contamination rates have estimated uncertainties on the order of ± 5 per cent and ± 2 per cent, respectively.

As can be seen, Table 2 shows that the sample produced from the selection criteria with an age < 14 d and brightening rate > 0.05 mag d^{-1} produces the largest YSN candidate sample. It contains 84 TNS classified YSNe (SNe selected before a phase of -10 d), with a further 57 YSNe from visual inspection of the unclassified objects' light curves. However, this sample is also the most contaminated, with non-YSN and non-SN contamination rates of 89 per cent and 33 per cent, respectively. In contrast, the smallest but least contaminated sample is that produced using the age and brightening rate criteria thresholds of 7 d and 0.2 mag d^{-1}, respectively. This sample contains 60 classified YSN and 17 visually identified YSNe, and has non-YSN and non-SN contamination rates of 71 per cent and 23 per cent, respectively.

More generally, Table 2 shows that the samples produced using the age constraint of 14 d contain more YSNe and SNe than those produced from the 7 d constraint. However, the samples

produced using the 14 d constraint are up to 2 per cent more contaminated, in terms of both non-YSN and non-SN contamination, than the corresponding samples produced with the 7 d constraint. Furthermore, the results in Table 2 show that as the brightening rate threshold value increases, the contamination and number of YSNe/SNe selected decreases.

2.3.4 Evaluation of selection criteria

From our results presented in Section 2.3.3, it is clear that the purest sample is that produced using the age and brightening rate thresholds of 7 d and 0.2 mag d^{-1}, respectively. As the aim of our selection criteria is to produce a pure sample of YSN, we select these thresholds for our YSN selection criteria. We will now discuss in more detail the YSN candidate sample produced using the age and brightening rate thresholds of 7 d and 0.2 mag d^{-1}, respectively. For simplicity, hereafter we refer to this sample and the selected thresholds as the YSN candidate sample and the YSN selection criteria, respectively.

Although our YSN candidate sample has the lowest contamination of the samples produced, it is still very contaminated with a non-YSN contamination of 71 per cent. The majority of the non-YSN contaminants are SNe that were selected after a phase of −10 d, accounting for 127 of the 187 contaminants (67.91 per cent). This is reflected in the non-SN contamination rate, which is only 23 per cent.

At a first glance a YSN candidate sample with a non-SN contamination rate of 23 per cent might seem to be too high to be worth implementing into a TiDES-like survey. However, this percentage does not quantify the number of fibre hours that would be spent on the YSN candidate sample contaminants. By calculating the wasted fibre hours as a percentage of TiDES's total fibre hours we can evaluate if this contamination level is too high or not. While we can calculate the number of fibre hours that would be wasted based on our ZTF YSN candidate sample, this would not be representative of the actual number that would be wasted during the operation of a TiDES-like survey. This is because TiDES-like surveys, and hence our selection criteria, will be selecting objects from LSST as opposed to ZTF. LSST will produce a much larger YSN candidate sample than that produced from the ZTF alerts. Therefore, we revisit this discussion of wasted fibre hours in Section 3.3.3, where we used the LSST simulations to produce a YSN candidate sample.

In addition to investigating the contamination of our YSN candidate sample, we also looked at the phase at which the SNe (both TNS classified SNe and SNe identified from our visual inspection) were selected by our selection criteria. Presented in Fig. 2 is the selected phase distribution of the SNe in our YSN candidate sample. It should be noted that the presented phases are not definitive phases, as they were calculated using estimates of the peak JDs of the SNe. As can be seen from Fig. 2, almost all of the SNe, with the exception of 7, were selected at pre-peak phases. However, only 77 of the 204 SNe (37.75 per cent) are YSNe, or in other words were selected before a phase of −10 d. This might seem like a low percentage of YSN, however, to fully evaluate our YSN selection criteria's performance we need to investigate how they perform when applied to LSST, which we present in Section 3.

3 APPLICATION OF YSN SELECTION CRITERIA TO LSST

To investigate the impact that our YSN selection criteria could have on a TiDES-like transient programme, we cannot use the ZTF alerts as they are not fully representative of the future LSST alerts that TiDES-like surveys will draw their targets from. Some of the differences between the two surveys that will affect our selection criteria and the resulting objects are as follows: LSST has different filter bands ($ugrizY$-bands), LSST has a much fainter limiting magnitude than ZTF, LSST will have a different observing strategy to that of ZTF, and LSST will observe SNe at a higher redshift distribution than ZTF. With this in mind, we adapted the ZTF developed YSN selection criteria for use with LSST data, evaluating their performance by applying them to an LSST simulation. Although there are many different LSST simulations that are suitable for use in this study, for example `PLAsTiCC` (R. Kessler et al. 2019) or `ELAsTiCC`,[7] we chose to use the simulations of CF. This was to allow for a direct comparison between our YSN selection criteria and those of TiDES (CF).

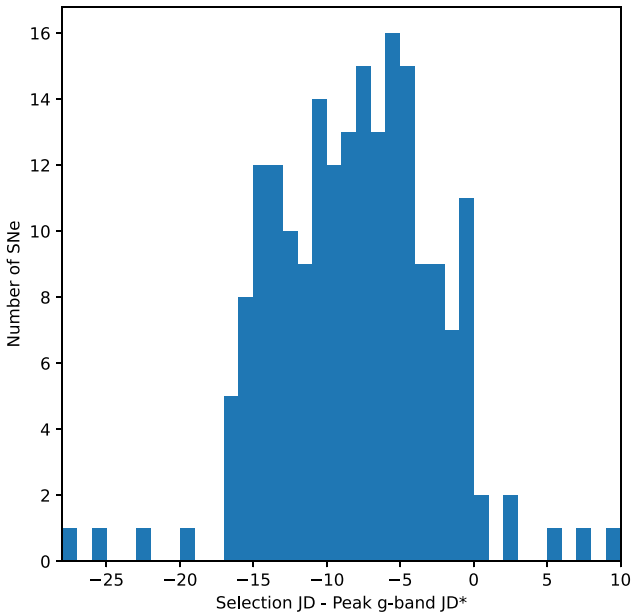

Figure 2. Phase distribution of the TNS classified and visually determined SNe in the sample that was produced by applying our YSN selection criteria (see Table 1), with age and brightening rate thresholds of 7 d and 0.2 mag d^{-1}, respectively, to 60 nights of ZTF transient alerts. Note that the phase has been truncated at −28 d.

3.1 Producing an LSST YSN candidate sample

3.1.1 Adaptation of ZTF developed YSN selection criteria

With the addition of the i, z, u, and Y- bands of LSST, we adapted the ZTF developed YSN selection criteria by including the LSST i- and z- bands. We did not include the u-band in our selection criteria as it is not often used by LSST and so our selection criteria will not benefit from including it. As we utilized the LSST simulation of CF, the Y band was also not included. This is due to the rest-frame Y-band being poorly defined in the spectrophotometric models that were used in this LSST simulation. To incorporate the i- and z-bands in our selection criteria, we included them in our applied magnitude criterion, as well as adapting our age and brightening rate criteria

[7]The DESC ELAsTiCC Challenge https://portal.nersc.gov/cfs/lsst/DESC_TD_PUBLIC/ELASTICC/ (accessed on 10/07/2025)

Table 3. Selection criteria that were applied to the LSST simulations of transient events to select YSNe. Provided are the criteria along with a description of their purpose. ∗ This criterion is not applied to the LSST simulations but will be applied to LSST live alerts in the future.

Criterion	Reasoning
g, r, i, or z-band magnitude < 22.5 mag	Ensures that the object will meet the TiDES SN SSC
$-70^\circ <$ Declination $< 5^\circ$	Extent of 4MOST declination range
Galactic latitude $< -10^\circ$ OR Galactic latitude $> 10^\circ$	Removal of Galactic transient sources
Number of g, r, i, or z-band $> 5\sigma$ positive difference detections ≥ 2	Two or more $> 5\sigma$ detections in a band required for brightening rate criterion
`Sherlock` classification not: VS, AGN, CV, BS ∗	Removal of contaminants
Age < 14 d	Removes older objects that are unlikely pre-peak SNe
Brightening rate > 0.2 mag d^{-1}	Removes dimming and slow brightening sources that are unlikely to be YSNe.

so that observations in the i- and z-bands are also considered if available.

One significant difference between ZTF and LSST will be the redshift (z) distribution of the observed transients. SNe in the ZTF sample typically have redshifts below 0.1, although there are some with redshifts up to 0.3 (M. Rigault et al. 2025). In contrast, the LSST SN redshift distribution should greatly exceed that of ZTF. For example, the LSST SN Ia distribution is estimated to peak at $z\sim0.5$, with some detected at redshifts beyond $z = 1$ (R. Kessler et al. 2019; V. Petrecca et al. 2024). Due to redshift distribution difference between ZTF and LSST, the brightening rate should be altered accordingly. For example, this could be achieved by applying the redshift correction given by equation (2):

$$\mathrm{BR_{LSST}} = \mathrm{BR_{ZTF}}/(1 + \mathrm{z_{LSST}}), \quad (2)$$

where BR is the brightening rate applied to either LSST or ZTF ($\mathrm{BR_{ZTF}} = 0.2$), and z_{LSST} is the average redshift of the LSST redshift distribution. An issue with adapting the brightening rate threshold based on the LSST SN redshift distribution is that it will be decreased. For example, if we assume $z_{\mathrm{LSST}} = 0.5$ then $\mathrm{BR_{LSST}}$ is 0.13. As we showed in Section 2.3.3, decreasing the brightening rate increases the contamination of the sample. Therefore, in the interest of producing a pure YSN sample, we do not adapt the brightening rate. This has the implication that our LSST selected YSN candidate sample will have a lower redshift distribution than if we were to adapt the brightening rate criterion.

Additionally, we applied a declination constraint of $-70^\circ <$ Dec $< 5^\circ$, so that only targets within the 4MOST footprint are selected from the LSST surveys. The adapted YSN selection criteria for LSST are stated, with reasoning, in Table 3. It is worth noting that the Sherlock classification criterion was not applied as it is only available through the Lasair broker. Regardless, we state this criterion in Table 3 as it should be applied to the future LSST live transient alerts to help exclude contamination from the produced YSN candidate sample.

3.1.2 *Applying the selection criteria*

With the criteria adapted for use with LSST, we applied them to the LSST simulation used by CF. This simulation utilizes the LSST baseline V3.4 simulation[8] and the *SuperNova ANAlysis* software (SNANA; R. Kessler et al. 2009) to produce a catalogue of SN events and photometry as would be observed by LSST over a 5 year period. The transients included in this simulation are SNe Ia, SNe Iax, SNe 91bg, SNe Ib, SNe Ic, SNe Ic-BL, SNe II, SNe IIb, SNe IIn, superluminous SNe (SLSNe), calcium rich transients (CART), and TDE. The simulations only include the LSST WFD and DDF surveys. The WFD survey covers an 18 000 deg^2 area that, under currently plans, will be observed using a rolling cadence[9] in $ugrizY$ filter bands down to a depth of 25 mag in the g-band (Ž. Ivezić & LSST Science Collaboration 2018). The DDF survey is a much smaller area survey consisting of five circular fields[10] of diameter $\sim3.5^\circ$ that will have a higher cadence and a deeper coverage than that of the WFD survey (Ž. Ivezić & LSST Science Collaboration 2018).

3.2 LSST YSN candidate samples

3.2.1 *LSST WFD survey*

Following the methods in Section 3.1, presented in Table 4 are the resulting samples of selected transients covering 5 yr of the LSST WFD survey. This shows the total number of objects simulated, the number of objects selected by our YSN selection criteria (YSN candidate sample). For comparison, we present the number of objects selected by the current TiDES selection criteria used by CF, hereafter referred to as the CF selection criteria and CF sample. We have also defined whether the objects were young (phase < -10 d), pre-peak (phase < 0 d), or post-peak (phase ≥ 0 d) at the time of selection. Note that YSNe are a subset of pre-peak SNe. The phase of selection was calculated using the peak date provided in the LSST simulation. As can be seen from Table 4, our YSN selection criteria selected 56 408 transients, of which 39 807 were young at the time of selection. The YSN candidate sample size is approximately only 7 per cent of the size of the current simulated CF sample, and contains 1 per cent of the total number of simulated WFD survey transients.

For each classification of transient within our sample, we present in Figs 3–6 and Appendix A comparisons between the selection phases for the samples produced by our selection criteria and the CF selection criteria. In general, the peak of the selection phase distributions produced from our selection criteria occur a few days before those produced by the CF selection criteria. For example, Fig. 3 shows that the SN Ia selection phase distribution produced by our YSN criteria peaks at ~ -14 d while the distribution produced by

[8] https://survey-strategy.lsst.io/index.html (accessed on 05/12/2024)

[9] LSST Survey Cadence Optimization Committee's Phase 2 Recommendations, available at https://pstn-055.lsst.io/ (accessed on 28/04/2025)

[10] Information of the 5th field: https://community.lsst.org/t/scoc-endorsement-of-euclid-deep-field-south-observations/6406 (accessed on 25/09/2024)

Table 4. Resulting number of transients selected from the 5 year LSST WFD survey simulation by our YSN selection criteria (stated in Table 3) and the CF selection criteria. Additionally, provided (in brackets) is the percentage of transients that were selected from the total number of LSST WFD survey simulated transients. Note that young transients are a subset of pre-peak transients.

Classification	Total simulated	5 Year WFD survey					
		YSN candidate sample			CF sample		
		Young	Pre-peak	Post-peak	Young	Pre-peak	Post-peak
		(< -10 d)	(< 0 d)	(≥ 0 d)	(< -10 d)	(< 0 d)	(≥ 0 d)
Ia	2 971 223	36 168 (1.22 per cent)	39 533 (1.33 per cent)	0 (0.00 per cent)	67 376 (2.27 per cent)	316 269 (10.64 per cent)	199 698 (6.72 per cent)
Iax	83 351	529 (0.63 per cent)	614 (0.74 per cent)	0 (0.00 per cent)	1514 (1.82 per cent)	5815 (7.00 per cent)	5105 (6.12 per cent)
91bg	69 266	513 (0.74 per cent)	2649 (3.82 per cent)	0 (0.00 per cent)	380 (0.55 per cent)	9664 (13.95 per cent)	10 956 (15.82 per cent)
Ib	89 365	515 (0.58 per cent)	675 (0.76 per cent)	0 (0.00 per cent)	2641 (2.96 per cent)	8095 (9.06 per cent)	7303 (8.17 per cent)
Ic	53 670	196 (0.37 per cent)	710 (1.32 per cent)	0 (0.00 per cent)	751 (1.40 per cent)	3734 (6.96 per cent)	5379 (10.02 per cent)
Ic-BL	34 511	141 (0.41 per cent)	344 (1.00 per cent)	51 (0.15 per cent)	217 (0.63 per cent)	1968 (5.70 per cent)	3896 (11.29 per cent)
II	782 637	4 (0.00 per cent)	2939 (0.38 per cent)	774 (0.10 per cent)	19 (0.00 per cent)	4741 (0.61 per cent)	74 885 (9.57 per cent)
IIb	220 409	1218 (0.55 per cent)	3891 (1.77 per cent)	962 (0.44 per cent)	2465 (1.12 per cent)	13 594 (6.17 per cent)	28 744 (13.04 per cent)
IIn	483 957	60 (0.01 per cent)	2561 (0.53 per cent)	105 (0.02 per cent)	3352 (0.69 per cent)	11 728 (2.42 per cent)	33 555 (6.93 per cent)
SLSN	32 922	285 (0.87 per cent)	301 (0.91 per cent)	0 (0.00 per cent)	7787 (23.65 per cent)	9709 (29.49 per cent)	8600 (26.12 per cent)
CART	16 719	30 (0.18 per cent)	141 (0.84 per cent)	10 (0.06 per cent)	96 (0.57 per cent)	589 (3.52 per cent)	1640 (9.81 per cent)
TDE	23 476	148 (0.63 per cent)	148 (0.63 per cent)	0 (0.00 per cent)	1409 (6.00 per cent)	2261 (9.63 per cent)	1523 (6.49 per cent)
Total	4 861 506	39 807 (0.82 per cent)	54 506 (1.12 per cent)	1902 (0.04 per cent)	88 007 (1.81 per cent)	388 167 (7.98 per cent)	381 284 (7.84 per cent)

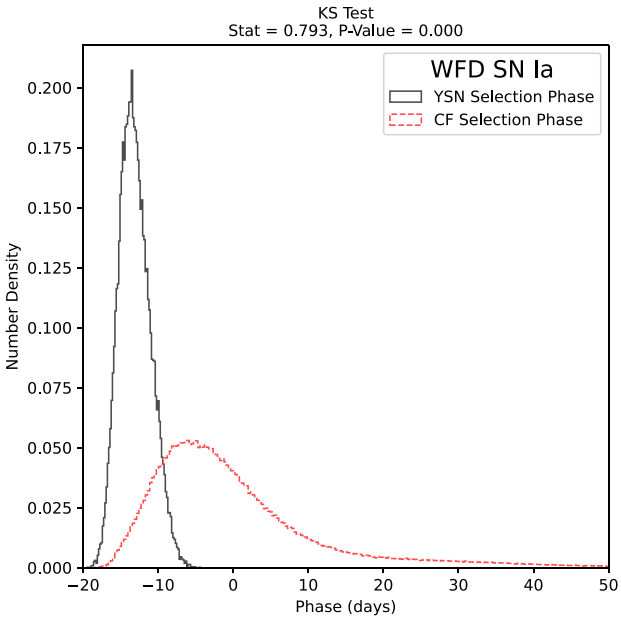

Figure 3. Comparison between the SN Ia selection phase distributions produced by applying our selection criteria (YSN; see Table 3) and the CF selection criteria to the LSST WFD survey simulation. Note that the distributions are normalized and that the phase has been truncated at 50 d.

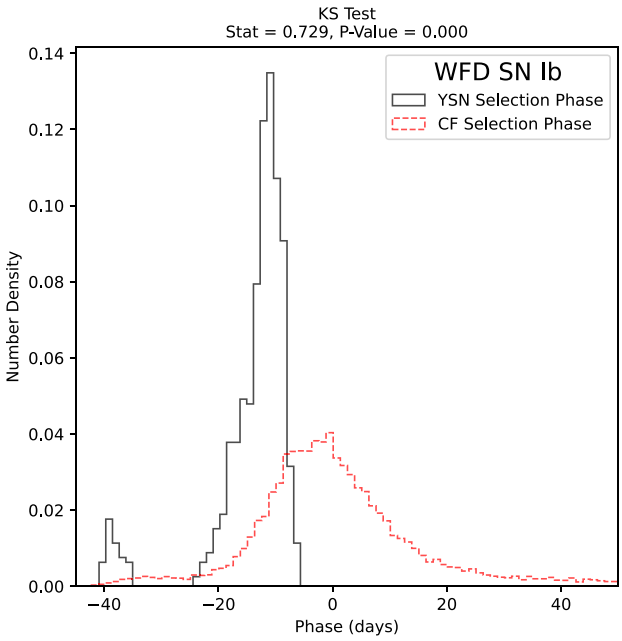

Figure 4. Comparison between the SN Ib selection phase distributions produced by applying our selection criteria (YSN; see Table 3) and the CF selection criteria to the LSST WFD survey simulation. Note that the distributions are normalized and that the phase has been truncated at 50 d.

the CF peaks at ~ -6 d. Furthermore, the two sided Kolmogorov–Smirnov (KS) tests performed on the YSN and CF phase distributions for each transient class all return P-values less than 0.0005, indicating that the two SN samples are drawn from different distributions.

For the majority of the transient classes, the selection phase distributions produced by our selection criteria are unimodal. However, for

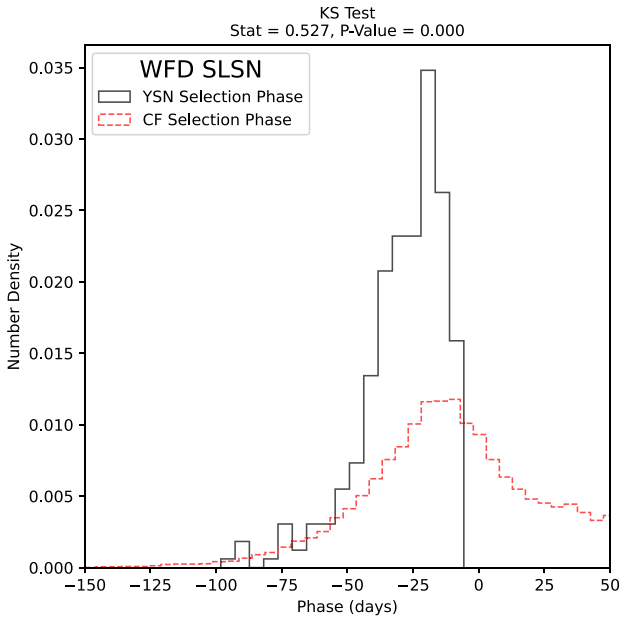

Figure 5. Comparison between the SLSN selection phase distributions produced by applying our selection criteria (YSN; see Table 3) and the CF selection criteria to the LSST WFD survey simulation. Note that the distributions are normalized and that the phase has been truncated at −150 and 50 d.

SNe Ib (Fig. 4) and SNe IIb (Fig. 6) their selection phase distributions display bimodality with the stronger of the peaks occurring ∼25 and ∼15 days after the weaker peaks, respectively. The weaker of the peaks occur at a phase of ∼ − 40 d for SNe Ib and ∼ − 15 d for SNe IIb. The cause of the bimodality in the SN IIb selection phase distribution is unclear. However, for the SN Ib distribution it arises due to the inclusion of SN 2005bf in the spectrophotometric templates used to simulate the transients in the LSST simulation. SN 2005bf is a transitional SN (Ib to Ic) and has a unique morphology, exhibiting two maxima separated by about 25 d and an unusually long rise to peak brightness of ∼40 d (G. Folatelli et al. 2006).

Lastly, the selection phase distributions produced by our selection criteria for many of the transient classes do not exceed into positive phases (post-peak), as is seen in Figs 3–5. However, for SNe II, IIb, IIn, and Ic-BL (see Fig. 6) the selection phase distributions extend up to phases of ∼7 d.

To gain a better understanding of the crossover between the objects selected by our YSN criteria and the CF criteria, we present in Table 5 the number of selected transients that are common to both sets of selection criteria. We also include the number of transients that are only selected by our selection criteria. As is seen, there are 38 657 SNe Ia and 15 787 non-SNe Ia that are commonly selected by both sets of selection criteria. Also indicated is that our selection criteria selects an additional 876 SNe Ia and 1088 non-SNe Ia that the CF selection criteria does not select.

Additionally, for each of the commonly selected LSST WFD survey transients, we compared the difference between their selection phases when selected by our YSN selection criteria and the CF criteria. Presented in Fig. 7 is the distribution of the selection phase differences. As is shown, the majority of transients (∼35 000) have a negative time difference, or in other words were selected by the YSN selection criteria before the CF selection criteria. As can be seen from Table 5, the commonly selected WFD transients are on average selected 3–5 d earlier by our YSN selection criteria.

3.2.2 LSST DDF survey

Following the methods presented in Section 3.1, presented in Table 6 are the resulting YSN candidate and CF samples of selected transients from the 5 year LSST DDF survey. As is shown, our YSN selection criteria selected 694 transients, of which only 31 were selected at post-peak phases and 547 were selected before a phase of −10 d (young). In contrast, the CF sample contains 7757 transients, of which 2922 were selected after peak brightness and 1433 were young at the time of selection.

To investigate if our selection criteria selects YSNe, we present in Figs 8–10 the selection phase distributions for SNe Ia, 91bg, and IIb that were produced by our selection criteria and the CF criteria. We present in Appendix B the phase distributions for the other classes of transients. However, it should be noted that the classes presented in Appendix B suffer from low number statistics and are only included for completeness.

Figs 8 and 9 show that for SNe Ia and 91bg-like SNe (a subset of SNe Ia) the selection phase distributions produced by our selection criteria are unimodal with peaks that occur approximately 5–10 d before those produced by the CF selection criteria. Furthermore, our selection criteria is shown to only select pre-peak SNe Ia and 91bg-like SNe, with a maximum selection phase of approximately −5 d. The two-sided KS tests performed on the distributions for the SNe Ia and 91bg both returned P-values less than 0.0005, indicating that the selection phase distributions of the YSN candidate and CF samples are drawn from different distributions.

In contrast, the SNe IIb selection phase distributions, presented in Fig. 10, show that our selection criteria produces a selection phase distribution that is bimodal, with the dominant peak occurring at a phase of ∼0, which is approximately the same as the selection phase distribution produced by the CF selection criteria. The secondary peak of the distribution occurs at a phase of ∼ − 15 d. As with the WFD SNe IIb, the cause of this bimodality unclear. The distribution displayed in Fig. 10 also shows that our selection criteria selects some (18 from Table 6) post-peak SNe IIb, with a maximum selection phase of ∼4 d.

As with the LSST WFD survey samples, to understand the crossover between the objects selected by our YSN selection criteria and the CF selection criteria, we present in Table 7 the number of selected transients that are common to both sets of selection criteria. We also include the number of transients that are only selected by our selection criteria. As is shown, there are 548 SNe Ia and 239 non-SNe Ia that are commonly selected. Our YSN selection criteria selects only 8 transients that were not selected by the CF selection criteria.

For the commonly selected LSST DDF survey transients, we directly compared the times at which they were selected by the two sets of selection criteria. Presented in Fig. 11 is the distribution of the time difference between when a commonly selected target was selected by our YSN selection criteria and the CF selection criteria. As indicated, approximately 600 of the commonly selected transients have a positive time difference (selected by the CF criteria first) up to a maximum of 4 d. The remaining ∼200 commonly selected transients are shown to have a negative time difference (selected by YSN criteria first) as low as −18 d.

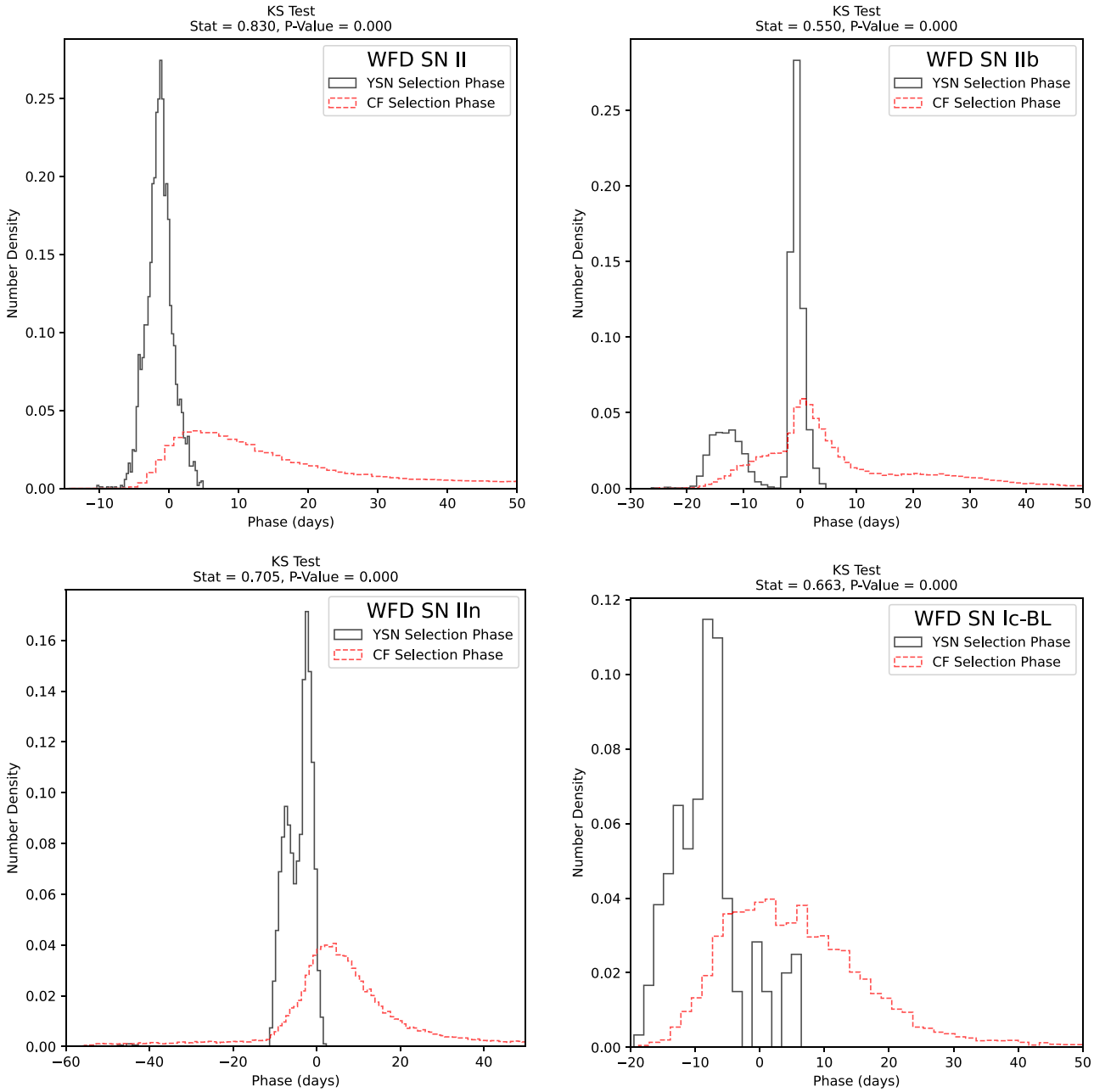

Figure 6. Comparison between the SN II, IIb, IIn, and IC-BL selection phase distributions produced by applying our selection criteria (YSN; see Table 3) and the CF selection criteria to the LSST WFD survey simulation. Note that the distributions are normalized and that all phases have been truncated at 50 d.

3.3 YSN selection criteria performance on LSST simulations

3.3.1 Sample size

From our results, presented in Section 3.2, it is evident from Tables 4 and 6 that our selection criteria produces a sample of transients that is not insignificant in number. From the 5 year LSST simulation, our YSN criteria selected a total of 56 408 WFD survey transients and 694 DDF survey transients for follow-up observations. However, our YSN candidate samples are much smaller than the samples produced by the CF selection criteria, with their WFD and DDF samples containing ∼14 and ∼11 times more transients, respectively. Although our YSN candidate sample of selected transients is smaller than the CF sample, the aim of our selection criteria is not to replace the current selection criteria of TiDES (CF criteria) or of a TiDES-like survey. Instead our YSN selection criteria are to be used in conjunction with the pre-existing selection criteria, with the aim of selecting some of the transients at earlier phases to enhance the YSN samples of TiDES-like surveys. With this in mind, the size of our YSN candidate sample indicates that incorporating our selection criteria into a TiDES-like survey has the potential to have a non-insignificant effect on the resulting SN sample.

Table 5. Number of LSST WFD simulated transients that were commonly selected by both our YSN selection criteria (see Table 3) and the CF selection criteria. Also included is the number of simulated transients that were only selected by our YSN criteria. Additionally, provided for the commonly selected transients are the average phases of selection by the CF criteria and our YSN criteria .

Classification	Commonly selected			YSN uniquely selected
	Quantity	Mean selection phase		
		CF	YSN	
Ia	38 657	−9 d	−13 d	876
Iax	604	−10 d	−14 d	10
91bg	2540	−5 d	−8 d	109
Ib	661	−10 d	−14 d	14
Ic	694	−6 d	−9 d	16
Ic-BL	383	−3 d	−8 d	12
II	3637	3 d	−1 d	76
IIb	4078	−1 d	−5 d	775
IIn	2598	−1 d	−4 d	68
SLSN	299	−21 d	−29 d	2
CART	148	−2 d	−6 d	3
TDE	145	−20 d	−25 d	3
Total	54 444			1964

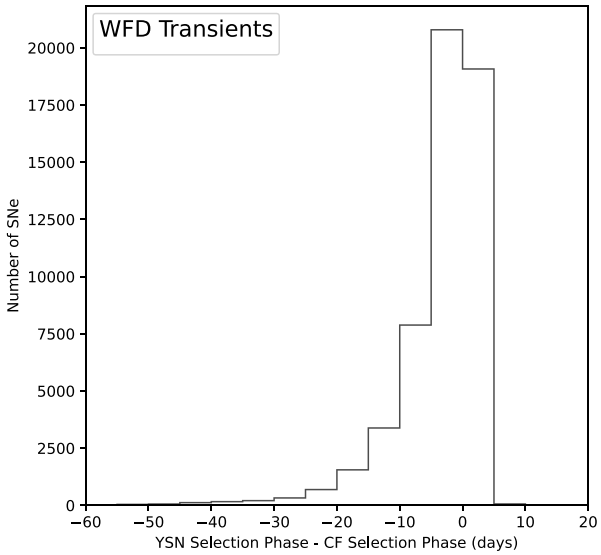

Figure 7. Distribution of the time differences of the selection of the LSST WFD transients that were selected by both our YSN selection criteria and the CF criteria. All of the simulated transient types (see Table 4) are included. Note that the phase difference has been truncated at −60 d.

3.3.2 Early selection effectiveness

Our results presented in Section 3.2, specifically Figs 3−6 and 8−10, showed that our selection criteria can select SN at earlier phases than the CF selection criteria. From Fig. 3, it is shown that for the LSST WFD SNe Ia the selection phase distribution produced by our selection criteria peaks approximately 10 d before the selection phase distribution produced by the CF selection criteria. This general trend is seen for all of the transient classes across both the WFD and DDF surveys (where there is no low number statistics), which indicates that our selection criteria on average selects younger objects that the CF criteria, therefore enhancing the early SN sample in the TiDES transient programme.

Table 6. Resulting number of transients selected from the 5 year LSST DDF survey simulation by our YSN selection criteria (stated in Table 3) and the CF selection criteria. Additionally, provided (in brackets) is the percentage of transients that were selected from the total number of LSST DDF survey simulated transients. Note that young transients are a subset of pre-peak transients.

Classification	Total simulated	5 Year DDF survey							
		YSN candidate sample				CF sample			
		Young	Pre-peak	Post-peak		Young	Pre-peak	Post-peak	
		(< −10 d)	(< 0 d)	(≥ 0 d)		(< −10 d)	(< 0 d)	(≥ 0 d)	
Ia	57 504	504 (0.88 per cent)	550 (0.96 per cent)	0 (0.00 per cent)		1223 (2.13 per cent)	3956 (6.88 per cent)	1352 (2.35 per cent)	
Iax	2384	5 (0.21 per cent)	6 (0.25 per cent)	0 (0.00 per cent)		21 (0.88 per cent)	63 (2.64 per cent)	48 (2.01 per cent)	
91bg	1532	6 (0.39 per cent)	31 (2.02 per cent)	0 (0.00 per cent)		7 (0.46 per cent)	142 (9.27 per cent)	84 (5.48 per cent)	
Ib	2558	2 (0.08 per cent)	5 (0.20 per cent)	0 (0.00 per cent)		27 (1.06 per cent)	96 (3.75 per cent)	43 (1.68 per cent)	
Ic	1665	2 (0.12 per cent)	9 (0.54 per cent)	0 (0.00 per cent)		9 (0.54 per cent)	44 (2.64 per cent)	55 (3.30 per cent)	
Ic-BL	797	3 (0.38 per cent)	8 (1.00 per cent)	1 (0.13 per cent)		4 (0.50 per cent)	26 (3.26 per cent)	26 (3.26 per cent)	
II	27 260	0 (0.00 per cent)	47 (0.17 per cent)	11 (0.04 per cent)		0 (0.00 per cent)	81 (0.30 per cent)	667 (2.45 per cent)	
IIb	5057	17 (0.34 per cent)	53 (1.05 per cent)	18 (0.36 per cent)		33 (0.65 per cent)	176 (3.48 per cent)	285 (5.64 per cent)	
IIn	9853	1 (0.01 per cent)	47 (0.48 per cent)	1 (0.01 per cent)		34 (0.35 per cent)	156 (1.58 per cent)	279 (2.83 per cent)	
SLSN	228	4 (1.75 per cent)	4 (1.75 per cent)	0 (0.00 per cent)		60 (26.32 per cent)	74 (32.46 per cent)	58 (25.44 per cent)	
CART	583	0 (0.00 per cent)	1 (0.17 per cent)	0 (0.00 per cent)		0 (0.00 per cent)	2 (0.34 per cent)	13 (2.23 per cent)	
TDE	293	3 (1.02 per cent)	3 (1.02 per cent)	0 (0.00 per cent)		15 (5.12 per cent)	19 (6.48 per cent)	12 (4.10 per cent)	
Total	109 714	547 (0.50 per cent)	663 (0.60 per cent)	31 (0.03 per cent)		1433 (1.31 per cent)	4835 (4.41 per cent)	2922 (2.66 per cent)	

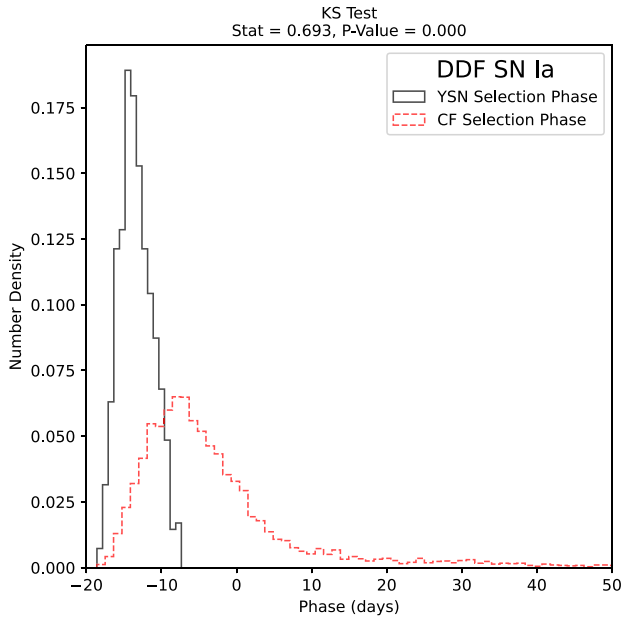

Figure 8. Comparison between the SN Ia selection phase distributions produced by applying our selection criteria (YSN; see Table 3) and the CF selection criteria to the LSST DDF survey simulation. Note that the distributions are normalized and that the phase has been truncated at 50 d.

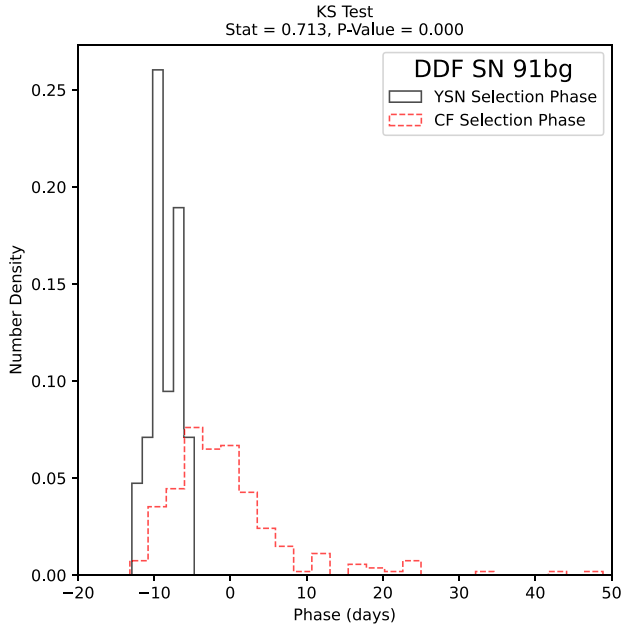

Figure 9. Comparison between the SN 91bg selection phase distributions produced by applying our selection criteria (YSN; see Table 3) and the CF selection criteria to the LSST DDF survey simulation. Note that the distributions are normalized and that the phase has been truncated at 50 d.

However, there are a two transient classes, SLSN and SN IIn, where the CF selection criteria can select the SN at earlier phases than our YSN criteria. While the phase distributions for these SN classes produced by our selection criteria have a peak at earlier phases, the CF criteria is able to select SLSN and SN IIn over 50 d earlier than our YSN criteria. This is demonstrated in Figs 5 and 6 (bottom left). For example, for the WFD survey SLSNe, the CF selection criteria was able to select them as early as ∼200 d before peak while our YSN selection criteria only selected them as early as ∼100 d before peak. However, these early detections are unrealistic, likely resulting from the over-extrapolation of the spectrophotometric templates used in the simulation of their LSST photometry. Although an artefact of the simulations, the earlier selection of transients by the CF criteria highlights that our selection criteria may not be optimized for each transient class. Specifically, transient types that exhibit an initial relatively slow phase of brightening in their early evolution, such as SLSNe, will not be selected at these early phases by our

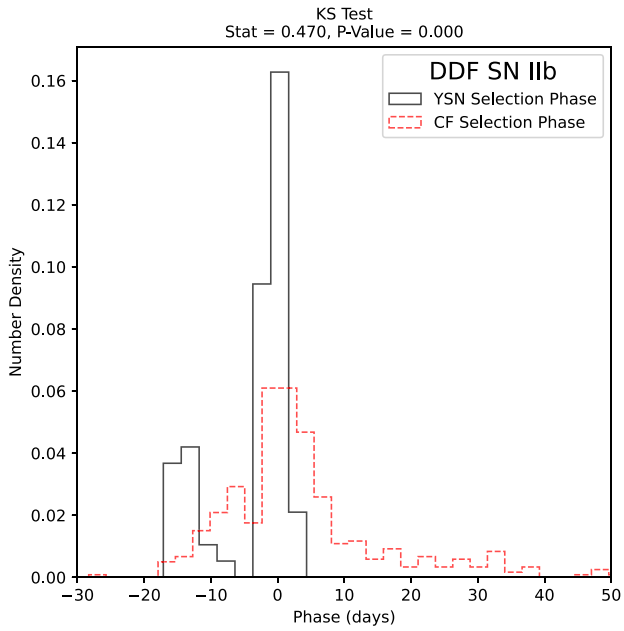

Figure 10. Comparison between the SN IIb selection phase distributions produced by applying our selection criteria (YSN; see Table 3) and the CF selection criteria to the LSST DDF survey simulation. Note that the distributions are normalized and that the phase has been truncated at 50 d.

Table 7. Number of LSST DDF simulated transients that were commonly selected by both our YSN selection criteria (see Table 3) and the CF criteria. Also included is the number of simulated transients that were only selected by our YSN criteria. Additionally, provided for the commonly selected transients are the average phases of selection by the CF criteria and our YSN criteria.

Classification	Commonly selected			YSN uniquely selected
	Quantity	Mean selection phase		
		CF	YSN	
Ia	548	−13 d	−13 d	2
Iax	6	−13 d	−14 d	0
91bg	31	−8 d	−9 d	0
Ib	5	−10 d	−10 d	0
Ic	8	−10 d	−10 d	1
Ic-BL	8	−7 d	−9 d	1
II	57	−1 d	−2 d	1
IIb	69	−3 d	−4 d	2
IIn	47	−5 d	−5 d	1
SLSN	4	−36 d	−36 d	0
CART	1	−3 d	−3 d	0
TDE	3	−27 d	−27 d	0
Total	787			8

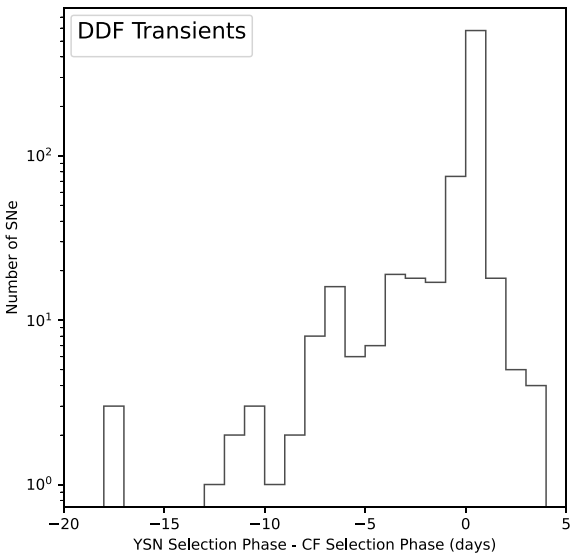

Figure 11. Distribution of the time differences of the selection of the LSST DDF transients that were selected by both our YSN selection criteria and the CF criteria. Note that all of the simulated transient types (see Table 4) are included.

YSN selection criteria due to the brightening rate criterion, which is designed to reject slowly brightening sources.

To gain a better understanding of how our YSN selection criteria performed, we compared the transients that were commonly selected by both the YSN and CF selection criteria. As shown by Figs 7 and 11, our YSN selection criteria was able to select ∼35000 WFD survey transients and ∼200 DDF survey transients at earlier times than the CF criteria. On average the commonly selected transients were selected by our YSN selection criteria 3-5 d earlier than the CF criteria, as is demonstrated by Table 5. Some of these transients were selected over 100 d earlier by our YSN selection criteria. This demonstrates that our YSN selection criteria can prove very useful for selecting transients at phases earlier than is currently possible with the CF criteria.

On the contrary, the CF selection criteria selected ∼19000 WFD and ∼600 DDF survey transients earlier than our YSN selection criteria. However, upon further investigation, most of these transients (with the exception of ∼4000) were selected within the same night but from observations taken at different times. Considering that TiDES-like surveys will not be able to follow-up a selected transient within the same night, due to there being no target of opportunity mode, a few hours difference between the YSN and CF selection criteria triggers will have no effect on when the selected SN could potentially be followed-up by a TiDES-like survey.

Investigating the remaining ∼4000 transients, it was found that the CF criteria selected many of them before our YSN criteria because they lacked multiple observations in same filter. At least two observations in a filter are required to calculate the brightening rate used in the YSN selection criteria, whereas the CF criteria does not require multiple observations in one filter and so can select some targets earlier than our YSN criteria. To solve this issue the brightening rate criterion could be removed from our selection criteria. However, the brightening rate criterion is used to limit the contamination that is selected. To retain the brightening rate and to allow for selection based on two detections in any filter, future works could investigate the use of cross-filter brightening rates.

Considering the improvements in earlier selection of ∼20000 SNe, we believe that our YSN selection criteria is suitable to be implemented in to a TiDES-like survey. However, we must finally consider the potential contamination of the YSN candidate sample in order to determine if we should implement our YSN selection criteria into TiDES or a TiDES-like survey.

3.3.3 Sample contamination

As previously discussed in Section 2.3.4, our YSN selection criteria should have a sufficiently high purity (low contamination). From our ZTF YSN candidate sample, we calculated that the non SN contamination of the sample was 23 per cent. However, we could not conclude if this level of contamination was sufficiently low to not waste too many fibre hours. By extrapolating the level of contamination from the ZTF YSN candidate sample to the LSST YSN candidate sample, we can estimate how many fibre hours a TiDES-like survey will potentially waste on non-SN sources.

From Tables 4 and 6, it is shown that the selected YSN candidate sample (WFD and DDF samples combined) contains 56 951 SNe (exclusion of TDE). Assuming that the contamination of the ZTF and LSST samples will be comparable, the number of non SN contaminants that would be selected as part of the LSST YSN candidate sample is 17 011 objects ($56951 \times 0.23/(1-0.23)$).

To estimate how many of the contaminants could be observed by a 4MOST/TiDES-like survey, we begin by making a few assumptions: 4MOST observes for on average 9 h per night (G. Guiglion et al. 2019), an average 4MOST pointing lasts 1 h, and 15 SNe are observed per 4MOST pointing. Based on these assumptions, a 4MOST-like survey can observe an estimated 135 SNe per night. 4MOST is a 5 year long survey, however, approximately 300 nights per year at Paranal are usable for observations (G. Guiglion et al. 2019), resulting in an estimated 1500 observable nights over the lifetime of 4MOST. As a result, an optimistic estimate suggests that a 4MOST-like survey could observe up to 202 500 SNe over its lifetime. This is much less than the total number of unique transients that are selected by our criteria and the CF criteria for follow-up with a 4MOST-like survey, which is approximately 780 000 transients. Therefore, up to ∼26 per cent of the selected samples can be estimated to be observed by a 4MOST-like survey, which means that ∼4423 ($17\,011 \times 0.26$) contaminants selected by our YSN selection criteria are observed over the lifetime of a TiDES-like survey.

By assuming that each observed object receives 40 min of observation time, over the lifetime of a TiDES-like survey (5 yr) the fibre hours wasted on the non-SN objects is ∼2949 h (40 min × 4423). This equates to approximately 1.2 per cent of TiDES's total available fibre hours (250 000 h (CF)) or 2.9 per cent of the fibre hours allocated for the TiDES SN survey (100 000 fibre hours, 40 per cent of the entirety of TiDES). We note here that these estimates are lower limits. This is due to our assumption that the contamination rate between LSST and ZTF will be comparable. Although this might be true in the later years of LSST, during the early stages the contamination rate will be elevated due to contaminating transients, such as AGN and CVs, being discovered for the first time. Based on our estimates of wasted fibre hours, we consider our selection criteria capable of producing a pure enough sample as to not waste too many fibre hours on non-SN targets.

4 OPTIMAL 4MOST-LIKE STRATEGY

The TiDES survey will spectroscopically follow-up transients that are selected from the LSST live transient alerts using 4MOST. As

of now, there is no coordination between the observing strategies of LSST and 4MOST, which results in an unknown variable delay between the selection of an LSST SN and its follow-up 4MOST observation. This leads to many cases where the SNR of a 4MOST observed SN spectrum is much lower than its highest obtainable SNR. Furthermore, the lack of coordination also negatively impacts our YSN selection criteria, as the unknown variable delay could be days, weeks, or even months, at which point a selected YSN has evolved and is likely no longer an early-time SN. To fully utilize our YSN selection criteria, follow-up of the targets should be conducted immediately. However, this is not possible with a 4MOST-like instrument due to the lack of a target of opportunity mode. Immediate follow-up of some targets could be conducted with dedicated target of opportunity programmes on instruments such as X-shooter (J. Vernet et al. 2011) or *Son-of-X-shooter* (SOXS; P. Schipani et al. 2016). However, these programmes would not provide the scale of observations that a TiDES-like survey could provide. Therefore, we propose to construct a 4MOST-like observing strategy for the case of maximizing transient follow-up.

To optimize a 4MOST-like observing strategy for the case of a TiDES-like survey and our YSN selection criteria, we propose that the 4MOST-like strategy follows (with some delay) the LSST observing strategy. In theory, this strategy would result in our LSST selected targets always being spectroscopically observed soon after their selection. This should increase the number of observed targets, improve the SN spectra SNR, and aid in obtaining early-time SN spectra. There are of course caveats to consider regarding the feasibility of a 4MOST-like survey following the strategy of LSST. For example, LSST will observe the southern sky approximately every 3 d,[11] which is not possible with a survey such as 4MOST, resulting in some LSST fields having to be skipped. As such, in this work we do not seek to construct a full 4MOST-like observing strategy, but instead we investigate and suggest guidelines for future works towards designing and simulating a full 4MOST-like observing strategy for time-domain science. Furthermore, we only investigate 4MOST-like strategies that cover the LSST WFD fields, as in the case of 4MOST the DDF fields will have a cadence based observing strategy based on requirements from the TiDES reverberation mapping survey (CF) and other 4MOST surveys.

4.1 Investigating observing strategies

4.1.1 Simulating 4MOST-like SN spectra

To simulate a SN spectrum as observed by a 4MOST-like instrument, for a given SN in the LSST simulation that was used in Section 3, we first created its template spectrum at a given phase. This was achieved by using the PYTHON package SNCOSMO (K. Barbary et al. 2024), which can extract a template spectrum from a spectrophotometric model for the given input parameters. Different models have different input parameters, for example SN Ia simulated with the extended SALT2 model (R. Hounsell et al. 2018) require the parameters of redshift, phase, SALT2 colour parameter, SALT2 stretch parameter, and apparent magnitude. Whereas a SN II simulated using the models of M. Vincenzi et al. (2019) requires only phase, redshift, and apparent magnitude. The spectrophotometric model and its input parameters for each of the SN in the LSST simulation are recorded in the simulation output files.

To the template spectra, we also applied the effect of Galactic extinction, which was achieved by using the SNCOSMO method `'F99Dust'` that applies the extinction model of E. L. Fitzpatrick (1999). We used the total-to-selective extinction ratio $R_V = 3.1$ and the extinction values defined for each SN in the LSST simulation output files. Although we included Galactic contamination in our SN spectral templates, we did not attempt to include contamination from the SNe's host galaxy.

With the template spectra created, we then simulated the effects of observing the SN spectra with 4MOST, which was accomplished by using the 4MOST exposure time calculator (ETC)[12] As we simulated observed spectra for a TiDES-like survey, we used the low-resolution spectrograph as this will be used by TiDES during operations (CF). For the observing conditions, we assumed the following typical observing conditions for TiDES targets: zenith angle of 45 deg, seeing of 0.8 arcsec, grey sky brightness, and an exposure time of 40 min. Although having constant observing conditions for all targets is unrealistic, varying the observing conditions would require development of a full 4MOST-like observing strategy, which is outside the scope of this work.

4.1.2 Applying an observing strategy

As previously mentioned, we investigated 4MOST-like WFD observing strategies that follow LSST with a delay time. To accomplish this, we applied our methods presented in Section 4.1.1 to the WFD CF and WFD YSN candidate samples produced and presented in Section 3, simulating their 4MOST observed spectra. To apply the 4MOST-like observing strategies with different delay times, we altered the phases at which the template spectra were created for. The phase that was used to produce a given SN's template spectrum is given as the phase at which the SN was selected plus the time delay of the 4MOST-like observing strategy. For example, an LSST SN selected at a phase of -10 d would be observed by a 4MOST-like strategy with a 3 d time delay at a phase of -7 d. Using these methods, we simulated the spectra for the LSST WFD selected CF and YSN candidate samples as if they had been observed using 4MOST-like observing strategies with delay times of 1, 3, 5, and 7 d.

4.1.3 Investigating observing strategy effects

To investigate the effects that the different time delays of the 4MOST-like observing strategy have on the resulting spectroscopically observed SN sample, we inspected the SNR of the spectra. Specifically, we analysed the observed SN samples' SNR distributions as well as the percentage of simulated SNe whose spectra exceed certain SNR thresholds. Following CF we chose to define the SNR of a spectrum as the mean SNR in 15 Å bins over the observer frame wavelengths 4500-8000 Å, hereafter denoted as $\mathrm{SNR}_{15\text{Å}}$. $\mathrm{SNR}_{15\text{Å}}$ thresholds of 5 and 3 were chosen as they can be used as a proxy for how reliably a SN spectrum can be classified. C. Balland et al. (2009) showed that spectra with a $\mathrm{SNR}_{15\text{Å}} > 5$ provide reliable classifications, while possible classifications were achievable for spectra with a $\mathrm{SNR}_{15\text{Å}}$ as low as 3. For the purpose of our study, using the SNR as a proxy for the reliability of the SN classifications is satisfactory. However, for a more in depth analysis of the SN classification reliability of 4MOST-like spectra, we refer the reader to A. Milligan et al. (2025). Although the chosen SNR thresholds are

[11] https://survey-strategy.lsst.io/baseline/wfd.html

[12] We used the `Python` API of the 4MOST ETC (https://escience.aip.de/readthedocs/OpSys/etc/master/index.html).

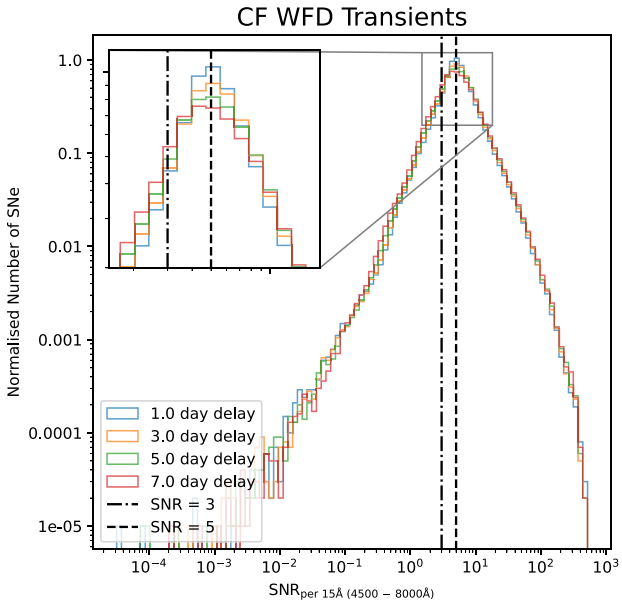

Figure 12. The CF LSST selected WFD SN sample's observed spectral SNR$_{15Å}$ distributions. The SNe were observed using 4MOST observing strategies that followed the LSST strategy by 1, 3, 5, and 7 d.

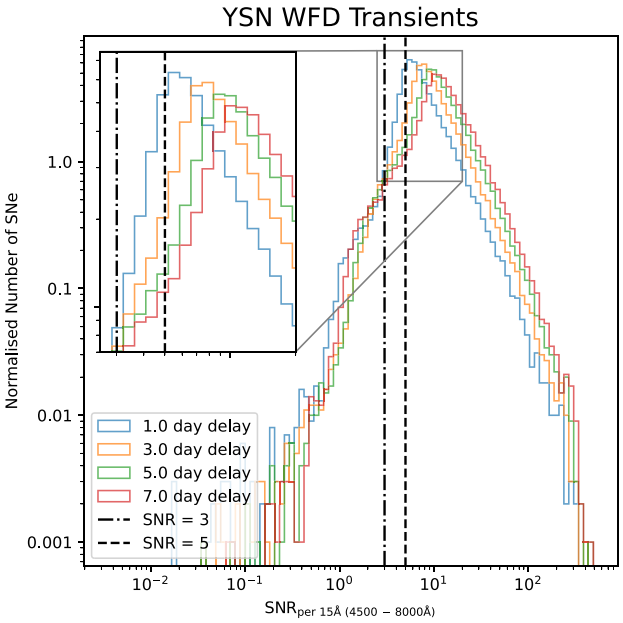

Figure 13. The LSST selected YSN candidate sample's observed spectral SNR$_{15Å}$ distributions. The SNe were observed using 4MOST observing strategies that followed the LSST strategy by 1, 3, 5, and 7 d.

Table 8. For both the LSST selected WFD SN samples (CF WFD and YSN WFD), presented are the percentages of 4MOST-like observed SNe whose spectra exceeded a SNR$_{15Å}$ of 5 or a SNR$_{15Å}$ of 3. These results are provided for the 4MOST-like observing strategies that follow the LSST strategy by delays of 1, 3, 5, and 7 d.

	WFD SN Sample			
4MOST-Like	CF		YSN Candidate	
Observing Strategies	SNR > 3	SNR > 5	SNR > 3	SNR > 5
1 d delay	81.2 per cent	50.8 per cent	94.1 per cent	75.0 per cent
3 d delay	79.7 per cent	51.5 per cent	95.1 per cent	85.6 per cent
5 d delay	77.8 per cent	50.1 per cent	94.9 per cent	87.5 per cent
7 d delay	75.2 per cent	47.7 per cent	94.2 per cent	87.7 per cent

a good proxy for spectra classifications, we also kept in mind that we want to maximize the spectra's SNR in order to reliably extract the spectral information required for performing astrophysical studies of SN.

4.2 Observed SN samples

4.2.1 CF sample

Following the methods of Section 4.1, we present in Fig. 12 the SNR distributions of the observed CF WFD SN sample's spectra following observations with the 4MOST-like strategies that follow the strategy of LSST with a 1, 3, 5, or 7 d delay. As is shown, the different observing strategies all produce similar SNR distributions that have no significantly notable differences. The SNR distributions of the 4MOST-like observed spectra all peak at a SNR$_{15Å}$ of 5 regardless of the 4MOST-like observing strategy.

In addition to the SNR$_{15Å}$ distributions, we present in Table 8 the percentage of transients whose observed 4MOST-like spectra exceed a SNR$_{15Å}$ of 5 or 3 when observed using the 4MOST-like observing strategies that follow the LSST strategy with a 1, 3, 5, and 7 d delay. From the table it is shown that of the SNe observed under any of the investigated 4MOST-like observing strategies, more than 47.7 per cent (75.2 per cent) of the observed CF WFD SNe have a SNR$_{15Å}$ > 5 (> 3). Table 8 also demonstrates that as the time delay between the LSST and 4MOST-like observing strategies increases, the percentage of observed CF WFD SNe with a SNR$_{15Å}$ > 3 decreases. This trend is not seen for the percentage of observed CF WFD SNe with a SNR$_{15Å}$ > 5, as the maximum percentage occurs with the 3 d delayed 4MOST observing strategy. The percentage of observed CF WFD SNe with a SNR$_{15Å}$ > 5 under the 3 d delayed strategy is 51.5 per cent, while the strategies with a 1, 3, and 7 d delays all have percentages that are more than 0.7 per cent less than the 3 d delay strategy.

4.2.2 YSN candidate Sample

As with the CF sample, we present in Fig. 13 the SNR distributions of the observed WFD YSN candidate sample's spectra following observations with the 4MOST-like strategies that follow the strategy of LSST with a 1, 3, 5, or 7 d delay. As is shown, the different observing strategies all produce similarly shaped SNR distributions. The peaks of the SNR distributions for the different observing strategies are shifted to higher SNR the larger the strategy's time delay is. For example, the WFD YSN candidate sample observed using the 7 d delayed 4MOST-like strategy peaks at a SNR$_{15Å}$ of ∼10, while the 1 d delayed strategy peaks at a SNR$_{15Å}$ of ∼6.

In addition, we also present in Table 8, the percentage of transients whose observed 4MOST-like spectra exceed a SNR$_{15Å}$ of 5 or 3 when observed using the 4MOST-like observing strategies that follow the LSST strategy with a 1, 3, 5, and 7 d delay. As the Table shows, the percentage of observed YSN WFD SN spectra whose SNR$_{15Å}$ is greater than 5 increases as the delay between the 4MOST-like and LSST observing strategies is increased, with 88.9 per cent of WFD YSN observed having a SNR$_{15Å}$ > 5 under the 7 d delayed 4MOST-like strategy. In contrast, the percentage of observed WFD YSN whose spectra have a SNR$_{15Å}$ > 3 is at maximum when the 4MOST-like 3 d delayed strategy is applied.

4.3 Discussion

4.3.1 CF sample

The results presented in Section 4.2.1, showed that the percentage of observed CF WFD SN whose spectra have a $SNR_{15Å} > 3$ decreases as the observing strategy time delay is increased from 1 d to 7 d. This suggests that a time delay of 1 d between the LSST and 4MOST-like observing strategies is the most optimal delay for obtaining the most spectra with a $SNR_{15Å} > 3$. On the contrary, the highest percentage of observed SN with a spectra whose $SNR_{15Å}$ is > 5 occurred when applying the 3 d delayed strategy, suggesting that this could be the more optimal strategy. However, we must also consider the significance of the $SNR_{15Å}$ thresholds of 5 and 3. As shown by C. Balland et al. (2009), SN spectra with a $SNR_{15Å} > 5$ can be reliable classified, while classifications from spectra with a $SNR_{15Å}$ as low as 3 are possible but less reliable.

Taking the significance of the SNR thresholds into consideration, using a 1 d delayed 4MOST-like observing strategy provides the highest percentage of observed SN that are likely to be classified, 81.2 per cent of the CF WFD sample. This is 1.5 per cent more than observed with the 3 d delayed strategy. However, the 3 d delayed 4MOST-like strategy provides the most spectra that could be reliably classified, 51.5 per cent of the CF WFD SN sample, which is 0.7 per cent more than observed with the 1 d delayed strategy.

For the case of the CF SN sample, to determine which strategy is optimal depends on if one values the prospect of obtaining more SN classifications over the reliability of the classifications. The TiDES SN survey values the reliability of the classifications and the physics that can be constrained from the spectra. Therefore, a 3 d delayed 4MOST-like observing strategy, which provides the highest percentage of spectra that can reliably classified ($SNR_{15Å} > 5$), is more optimal for the CF SN sample.

4.3.2 YSN candidate sample

The results presented in Section 4.2.2 showed that the SNR distribution is shifted to higher SNR as the delay time is increased. This can be explained by the fact that our YSN objects are predominantly selected at pre-peak phases. As the 4MOST-like observing strategy time delay is increased, the number of SNe that evolve to near peak brightness increases, resulting in an increase in the number of SNe that are bright enough such that their spectral $SNR_{15Å} > 5$. From the observing strategies investigated, the longest delay of 7 d produces the highest percentage (87.7 per cent) of SNe that have good quality spectra ($SNR_{15Å} > 5$). Although this strategy is the most optimal for obtaining good quality spectra, it is counterproductive for observing early-time SN spectra.

For a TiDES-like survey to fully capitalize on the earlier SN selection provided by our YSN selection criteria, quick follow up of the YSN targets is required. Ideally an event would be followed up within minutes of selection, however, this is not possible for a TiDES-like survey as there is no target of opportunity mode. Therefore, a 4MOST-like observing strategy that follows the LSST observing strategy with a delay of 1 d is most optimal for making the most out of our YSN selection criteria's early triggers. One limitation of this strategy, as shown by our results in Section 4.2.2, is that it produces the lowest percentage of SNe with good quality spectra, at 12.7 per cent less than the most optimal strategy (7 d delay strategy). However, the percentage of SNe for which a possible classification is achievable (spectrum $SNR_{15Å} > 3$) is 94.1 per cent, which is at most 1.0 per cent less than the other observing strategies investigated, and only 0.1 per cent less than the 7 d delayed observing strategy.

5 CONCLUSIONS

We have developed a set of selection criteria for TiDES-like surveys that will select YSNe from the LSST live transient alerts for spectroscopic follow-up. The aim of our selection criteria was to enhance the YSN samples of TiDES-like surveys by selecting transient events sooner than a TiDES-like selection criteria, potentially allowing for observations of SN spectra at earlier phases.

To develop our selection criteria, we first utilized the transient alerts from ZTF, allowing us to develop a set of selection criteria that could produce a candidate sample of YSN (SNe selected before a phase of -10 d) that was not overly contaminated with non-SN transients, and spurious transient alerts. By applying our selection criteria to the ZTF alerts over a period of 60 nights, we produced a YSN candidate sample consisting of 60 classified YSNe and 17 unclassified but likely YSNe. The non SN contamination of our produced ZTF YSN candidate sample was 23 per cent.

To evaluate the effect that our selection criteria could have on a TiDES-like SN survey, we exploited the LSST simulations of CF, producing an LSST YSN candidate sample by applying the following ZTF developed YSN selection criteria:

(i) Consider only LSST $griz$ bands.
(ii) Object is brighter than 22.5 mag in any $griz$-bands.
(iii) Object's declination is between 5° and -70°.
(iv) Object's Galactic latitude is not between -10° and 10°.
(v) Object has two or more $> 5\sigma$ detections in a given filter.
(vi) Object has no previous detections more than 7 d before the latest detection.
(vii) Brightening rate in any $griz$-band > 0.2 mag d^{-1}.

In total our YSN selection criteria produced an LSST selected SN sample consisting of 56 408 WFD survey transients and 694 DDF survey transients. Although this sample is significantly smaller than the CF sample (857 458 WFD survey and 9190 DDF survey transients), our selection criteria were developed to select early transients rather than produce a large sample, and is intended to be applied in conjunction with existing selection criteria such as those used by TiDES (CF). We demonstrated that our YSN selection criteria can provide earlier selection of LSST observed SNe, allowing TiDES-like surveys to enhance their early SN science capabilities.

In addition, we also showed that our selection criteria is capable of producing a YSN candidate sample that is sufficiently pure. By extrapolating the contamination rate from the ZTF sample (23 per cent) and estimating the maximum possible number of SNe that a TiDES-like survey could observe over its lifetime, we estimated (as a lower limit) that 2949 fibre hours (1.2 per cent of TiDES's total fibre hours) will be wasted over a 5 yr survey. We believe that the number of fibre hours spent on non-SN sources is low enough such that it will not have a significant negative impact on a TiDES-like survey, especially when considering the earlier selection benefit that is gained by our YSN selection criteria.

Finally, we investigated different 4MOST-like observing strategies to optimize the output of a TiDES-like survey and our YSN criteria. Specifically, we investigated simplistic 4MOST-like observing strategies that follow the strategy of LSST with delays of 1, 3, 5, and 7 d, looking only at the LSST WFD fields. For the CF sample, our results showed that the 3 day delayed 4MOST-like strategy was the most optimal strategy, as it provided the highest number of spectra (51.5 per cent of observed WFD SNe) that can be reliably

classified ($SNR_{15Å} > 5$). However, this was not replicated for the YSN candidate sample, as the 7 d delayed strategy provided the most spectra that can be reliably classified. We did not consider the 7 d delayed 4MOST-like strategy to be optimal for the YSN candidate sample due to the relatively long delay, which would counteract the early SN triggers. Instead, we considered the 1 d delayed strategy to be the most optimal strategy for the YSN candidate sample, as it provides the quickest follow-up. Although we showed that this strategy produced the lowest percentage of good quality spectra (spectra with a $SNR_{15Å} > 5$), the percentage of good quality spectra is still relatively high at 75.0 per cent. Therefore, the 4MOST-like observing strategy that follows the LSST strategy with a 1 d delay is most optimal for the YSN candidate sample and the resulting early-time SN science.

In summary, this work has demonstrated the benefits that a TiDES-like survey can gain by implementing our YSN selection criteria alongside its own selection criteria. Specifically, we have shown that our YSN criteria will enhance the early-time science capabilities of a TiDES-like survey. Furthermore, we recommend that future work towards designing and simulating a 4MOST-like observing strategy should adopt a strategy that closely follows the LSST strategy with a delay of 3 d or a delay of 1 d for optimizing the CF sample or the YSN candidate sample, respectively.

ACKNOWLEDGEMENTS

The authors thank Mathew Smith for their assistance with the simulations, Mark Sullivan for discussions and comments on earlier drafts of this work, and Alexander Fritz for their comments. Extensive use of PYTHON was used during this work, specifically the packages: NUMPY (C. R. Harris et al. 2020), ASTROPY (Astropy Collaboration et al. 2013, 2018, 2022), and MATPLOTLIB (J. D. Hunter 2007). This work was supported by the Science and Technology Facilities Council (STFC) grant ST/X508810/1. KM acknowledges funding from EU H2020 ERC grant no. 758638 and Horizon Europe ERC grant no. 101125877. IH acknowledges support from STFC through grants ST/Y001230/1 and ST/V000713/1, and a Leverhulme Trust International Fellowship, reference IF-2023-027. SJS acknowledges funding from STFC grants ST/Y001605/1, ST/X006506/1, ST/T000198/1, a Royal Society Research Professorship and the Hintze Charitable Foundation.

DATA AVAILABILITY

All data are available upon reasonable request to the corresponding author.

REFERENCES

Arnett W. D., 1969, Ap&SS, 5, 180
Astropy Collaboration et al., 2013, A&A, 558, A33
Astropy Collaboration et al., 2018, AJ, 156, 123
Astropy Collaboration et al., 2022, ApJ, 935, 167
Balland C. et al., 2009, A&A, 507, 85
Barbary K. et al., 2025, SNCosmo. Zenodo,
Bellm E. C. et al., 2019, PASP, 131, 018002
Ben-Ami S., Konidaris N., Quimby R., Davis J. T., Ngeow C. C., Ritter A., Rudy A., 2012, in McLean I. S., Ramsay S. K., Takami H. eds, Proc. SPIE Conf. Ser. Vol. 8446, Ground-based and Airborne Instrumentation for Astronomy IV. Bellingham, SPIE, p. 844686
Bianco F. B. et al., 2011, ApJ, 741, 20
Blagorodnova N. et al., 2018, PASP, 130, 035003
Boos S. J., Townsley D. M., Shen K. J., 2024, ApJ, 972, 200
Bruch R. J. et al., 2023, ApJ, 952, 119
Burke J. et al., 2022a, ApJ, 994, 87
Burke J., Howell D. A., Sand D. J., Hosseinzadeh G., 2022b, preprint (arXiv:2208.11201)
Deckers M. et al., 2022, MNRAS, 512, 1317
Di Stefano R., Voss R., Claeys J. S. W., 2011, ApJ, 738, L1
Dong Y. et al., 2024, ApJ, 974, 316
Fausnaugh M. M. et al., 2023, ApJ, 956, 108
Fink M., Hillebrandt W., Röpke F. K., 2007, A&A, 476, 1133
Fink M., Röpke F. K., Hillebrandt W., Seitenzahl I. R., Sim S. A., Kromer M., 2010, A&A, 514, A53
Fink M. et al., 2014, MNRAS, 438, 1762
Firth R. E. et al., 2015, MNRAS, 446, 3895
Fitzpatrick E. L., 1999, PASP, 111, 63
Folatelli G. et al., 2006, ApJ, 641, 1039
Fremling C. et al., 2020, ApJ, 895, 32
Frohmaier C. et al., 2025, ApJ, 992, 158 (CF)
Gagliano A. et al., 2022, ApJ, 924, 55
Gal-Yam A. et al., 2014, Nature, 509, 471
Gamezo V. N., Khokhlov A. M., Oran E. S., 2005, ApJ, 623, 337
Ganeshalingam M., Li W., Filippenko A. V., 2011, MNRAS, 416, 2607
Guiglion G. et al., 2019, The Messenger, 175, 17
Hallakoun N., Maoz D., 2019, MNRAS, 490, 657
Harris C. R. et al., 2020, Nature, 585, 357
Hayden B. T. et al., 2010, ApJ, 712, 350
Hounsell R. et al., 2018, ApJ, 867, 23
Hunter J. D., 2007, Computing in Science and Engineering, 9, 90
IAU, 2026, Transient Name Server, https://www.wis-tns.org/ (20/10/2023)
Iben I. J., Tutukov A. V., 1984, ApJ, 284, 719
Ivezić Ž., LSST Science Collaboration, 2018, The LSST System Science Requirements Document. Available at https://docushare.lsst.org/docushare/dsweb/Get/LPM-17 (26/03/2023)
Ivezić Ž. et al., 2019, ApJ, 873, 111
Jacobson-Galán W. V. et al., 2023, ApJ, 954, L42
de Jong R. S. et al., 2019, Messenger, 175, 3
Jordan IV G. C., Perets H. B., Fisher R. T., van Rossum D. R., 2012, ApJ, 761, L23
Kasen D., 2010, ApJ, 708, 1025
Kessler R. et al., 2009, PASP, 121, 1028
Kessler R. et al., 2019, PASP, 131, 094501
Khazov D. et al., 2016, ApJ, 818, 3
Khokhlov A. M., 1991, A&A, 245, 114
Kochanek C. S., 2019, MNRAS, 483, 3762
Kozyreva A., Klencki J., Filippenko A. V., Baklanov P., Mironov A., Justham S., Chiavassa A., 2022, ApJ, 934, L31
Kromer M., Sim S. A., Fink M., Röpke F. K., Seitenzahl I. R., Hillebrandt W., 2010, ApJ, 719, 1067
Kromer M. et al., 2013, MNRAS, 429, 2287
Kushnir D., Katz B., Dong S., Livne E., Fernández R., 2013, ApJ, 778, L37
Lach F., Callan F. P., Bubeck D., Röpke F. K., Sim S. A., Schrauth M., Ohlmann S. T., Kromer M., 2022, A&A, 658, A179
Magee M. R., Maguire K., Kotak R., Sim S. A., 2021, MNRAS, 502, 3533
Masci F. J. et al., 2019, PASP, 131, 018003
Miller A. A. et al., 2020, ApJ, 902, 47
Milligan A. et al., 2025, MNRAS, 543, 247
Ni Y. Q. et al., 2025, ApJ, 983, 3
Noebauer U. M., Kromer M., Taubenberger S., Baklanov P., Blinnikov S., Sorokina E., Hillebrandt W., 2017, MNRAS, 472, 2787
Nomoto K., Thielemann F. K., Yokoi K., 1984, ApJ, 286, 644
Ogawa M., Maeda K., Kawabata M., 2023, ApJ, 955, 49
Pastorello A. et al., 2007, Nature, 447, 829
Patterson M. T. et al., 2019, PASP, 131, 018001
Petrecca V. et al., 2024, A&A, 686, A11
Piro A. L., Morozova V. S., 2016, ApJ, 826, 96
Polin A., Nugent P., Kasen D., 2019, ApJ, 873, 84
Rabinak I., Livne E., Waxman E., 2012, ApJ, 757, 35
Riess A. G. et al., 1999, AJ, 118, 2675
Rigault M. et al., 2019, A&A, 627, A115

Rigault M. et al., 2025, A&A, 694, A1
Röpke F. K., Niemeyer J. C., 2007, A&A, 464, 683
Schipani P. et al., 2016, in Evans C. J., Simard L., Takami H. eds, Proc. SPIE Conf. Ser. Vol. 9908, Ground-based and Airborne Instrumentation for Astronomy VI. SPIE, Bellingham, p. 990841
Seitenzahl I. R. et al., 2013, MNRAS, 429, 1156
Shen K. J., Moore K., 2014, ApJ, 797, 46
Smith K. W. et al., 2019, Research Notes of the American Astronomical Society, 3, 26
Smith N. et al., 2007, ApJ, 666, 1116
Smith N., Pearson J., Sand D. J., Ilyin I., Bostroem K. A., Hosseinzadeh G., Shrestha M., 2023, ApJ, 956, 46
Soker N., 2013, in Di Stefano R., Orio M., Moe M., eds, IAU Symposium, Vol. 281, Binary Paths to Type Ia Supernovae Explosions. Cambridge University Press, Cambridge, p. 72
Swann E. et al., 2019, The Messenger, 175, 58
Vernet J. et al., 2011, A&A, 536, A105
Vincenzi M., Sullivan M., Firth R. E., Gutiérrez C. P., Frohmaier C., Smith M., Angus C., Nichol R. C., 2019, MNRAS, 489, 5802
Wang B., Zhou W. H., Zuo Z. Y., Li Y. B., Luo X., Zhang J. J., Liu D. D., Wu C. Y., 2017, MNRAS, 464, 3965
Whelan J., Iben Icko J., 1973, ApJ, 186, 1007
Williams R. D., Francis G. P., Lawrence A., Sloan T. M., Smartt S. J., Smith K. W., Young D. R., 2024, RAS Techniques and Instruments, 3, 362
Yaron O. et al., 2017, Nature Physics, 13, 510
Young D. R., 2023, Sherlock. Zenodo,
Zimmerman E. A. et al., 2024, Nature, 627, 759

APPENDIX A: LSST WFD SELECTION PHASE DISTRIBUTIONS

Presented are the WFD survey transients' selection phase distributions produced by applying our YSN selection criteria and the CF selection criteria to the simulated LSST WFD survey. Only the transient classes not presented in the main body are included here. Note that the distributions are normalized and that the phases have been truncated at 50 d.

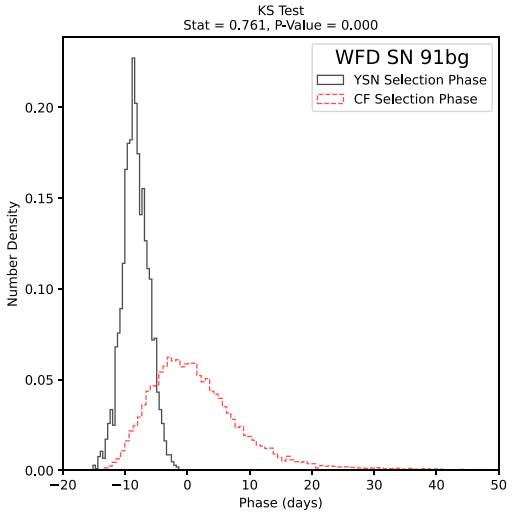
KS Test
Stat = 0.761, P-Value = 0.000
WFD SN 91bg
YSN Selection Phase
CF Selection Phase
Number Density
Phase (days)

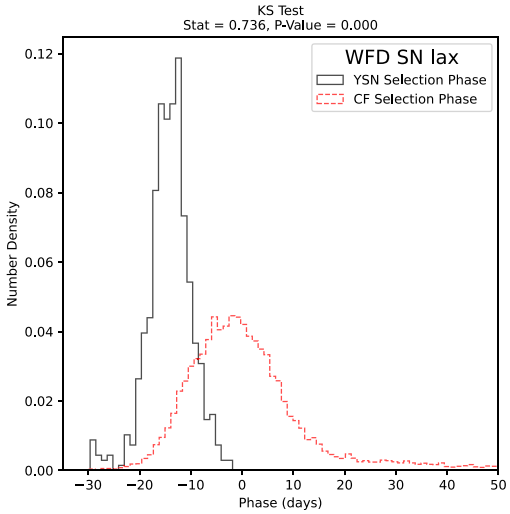
KS Test
Stat = 0.736, P-Value = 0.000
WFD SN Iax
YSN Selection Phase
CF Selection Phase
Number Density
Phase (days)

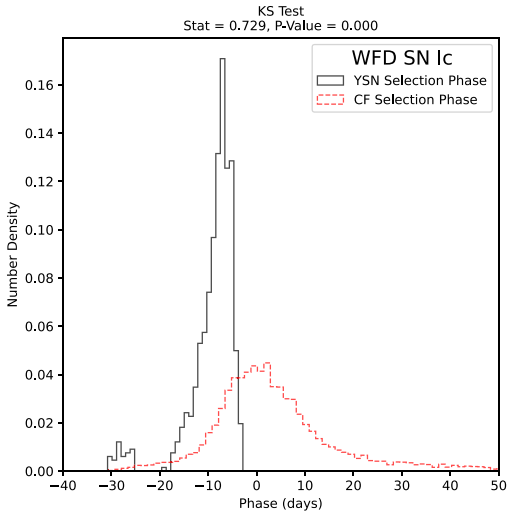
KS Test
Stat = 0.729, P-Value = 0.000
WFD SN Ic
YSN Selection Phase
CF Selection Phase
Number Density
Phase (days)

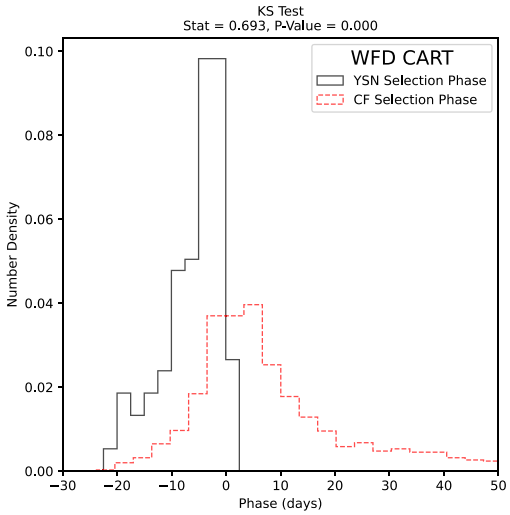
KS Test
Stat = 0.693, P-Value = 0.000
WFD CART
YSN Selection Phase
CF Selection Phase
Number Density
Phase (days)

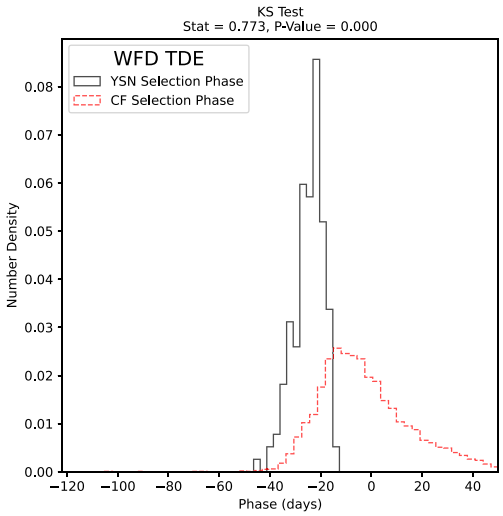
KS Test
Stat = 0.773, P-Value = 0.000
WFD TDE
YSN Selection Phase
CF Selection Phase
Number Density
Phase (days)

APPENDIX B: LSST DDF SELECTION PHASE DISTRIBUTIONS

Presented are the DDF survey transients' selection phase distributions produced by applying our YSN selection criteria and the CF selection criteria to the simulated LSST DDF survey. Only the transient classes not presented in the main body are included here. Note that the distributions are normalized and that the phases have been truncated at 50 d.

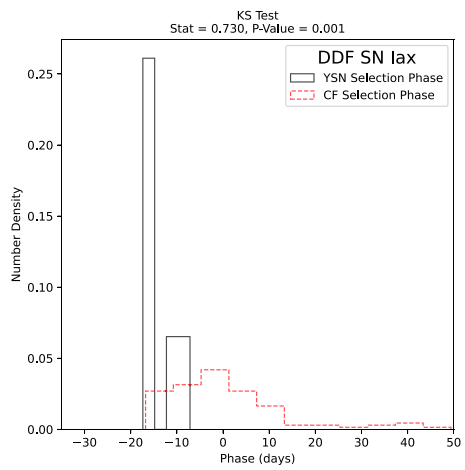

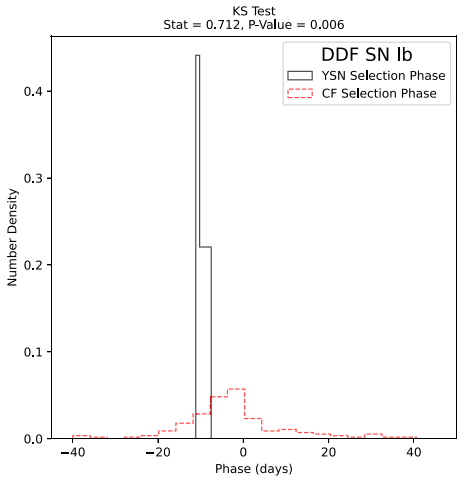

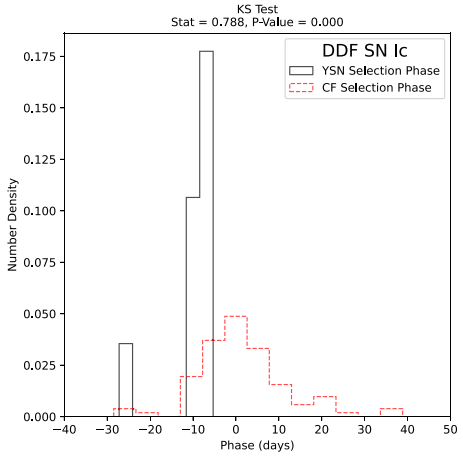

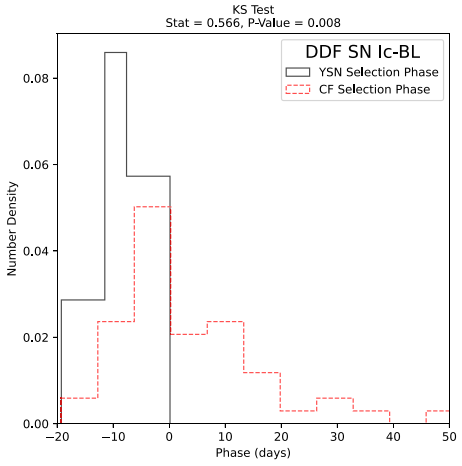

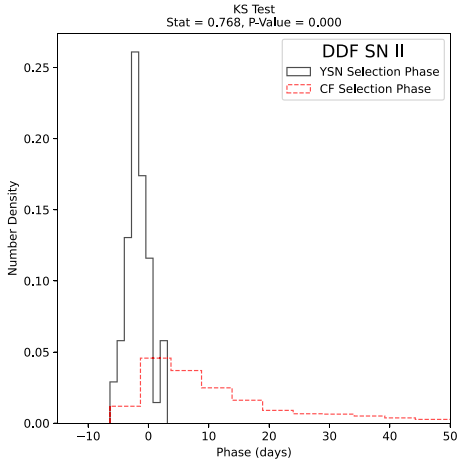

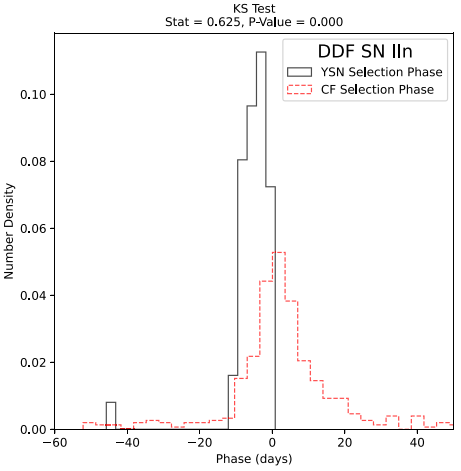

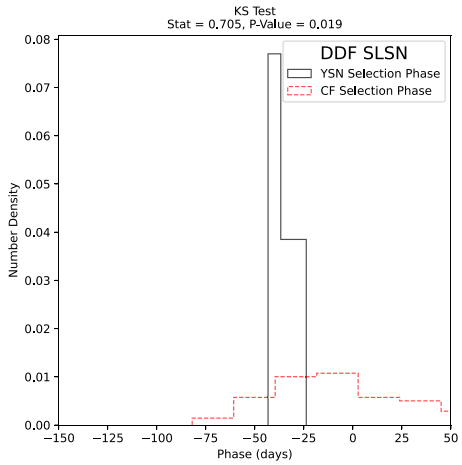

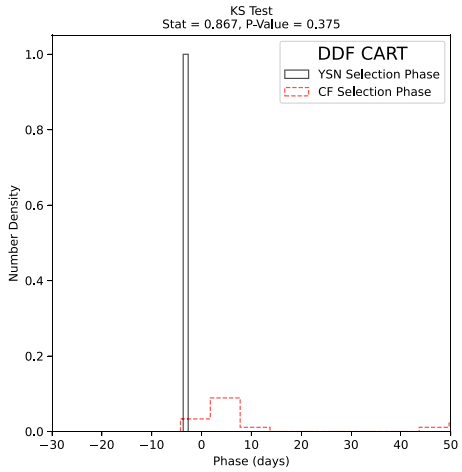

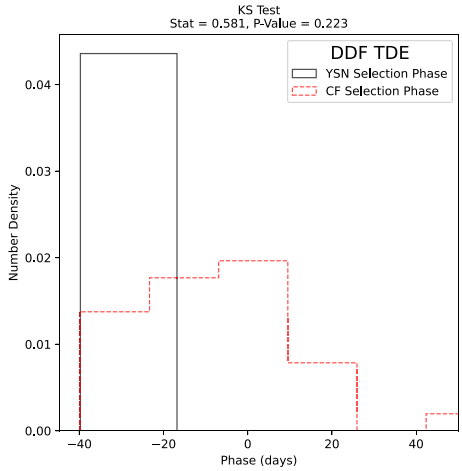

This paper has been typeset from a TEX/LATEX file prepared by the author.